AN OPEN SURFACE INTEGRAL FORMULATION FOR ELECTROMAGNETIC SCATTERING BY A MATERIAL PLATE

DISSERTATION

Presented in Partial Fulfillment of the Requirements for the Degree Doctor of Philosophy in the Graduate School of The Ohio State University

By

Mark Richard Schrote, B.S.E.E., M.Sc.

*****

The Ohio State University

1983

Reading Committee:

Professor C.H. Walter

Professor W.D. Burnside

Professor D.L. Moffatt

Approved By

Adviser

Department of Electrical Engineering

ACKNOWLEDGMENT

The author would like to express his thanks to his Graduate Adviser, Professor C.H. (Buck) Walter. Special thanks must be given to Dr. E.H. Newman, who contributed much to this study. The experience of working with and the worldly wisdom of Dr. Newman has left a lasting impression on the author. Acknowledgment must also be given to Professor Jack Richmond for his helpful discussions. Finally, the author would like to convey his appreciation to the Joint Services Electronics Program, who supported this work financially.

VITA

July 16, 1956	Born - Marion, Ohio
1978	B.S.E.E., Ohio State University, Columbus, Ohio
1980	M.Sc., The Ohio State University, Columbus, Ohio
1978-present	Graduate Research Associate, The Ohio State University ElectroScience Laboratory, Department of Electrical Engineering

PUBLICATIONS

"Some Effects of the Circumferential Polarization of Current on Thin-Wire Antennas", (co-authors, E.H. Newman, A.R. Djordjevic, B.D. Popovic and M.B. Dragovic), IEEE Trans. on Antennas and Prop., Vol. AP-29, pp. 815-817, September 1981.

"A Wide Band Electrically Small Superdirective Array", (co-author, E.H. Newman), IEEE Trans. on Antennas and Prop., Vol. AP-30, pp. 1172-1176, November 1982.

"On the Current Distribution for Open Surfaces", (co-author, E.H. Newman), IEEE Trans. on Antennas and Prop., Vol. AP-31, pp. 515-518, May 1983.

FIELDS OF STUDY

Major Field: Electrical Engineering

Studies in Antenna Theory. Professor C.H. Walter

Studies in Electromagnetic Theory. Professor R.G. Kouyoumjian

Studies in Communication Theory. Professor D.T. Davis

Studies in Mathematics. Professor S. Drobot

Studies in Physics. Professor R.G. Seyler

TABLE OF CONTENTS

LIST OF FIGURES

CHAPTER I

INTRODUCTION

The problem of evaluating the electromagnetic fields scattered by material objects has received increased attention in recent years. The use of non-metallic plates is increasing, particularly in aircraft, where they are used to reduce weight and to modify the radar cross section (RCS). Estimates predict that aircraft designed between 1985 and 1995 will be 65% composite material by weight [1].

This dissertation presents a technique for the analysis of electromagnetic scattering from a thin material plate. The two types of material plates studied in this dissertation are: (1) small but finitely thick three-dimensional planar slabs composed of some dielectric/ferrite medium and (2) infinitesimally thin and pefectly conducting plates coated on one or both sides by an electrically thin dielectric/ferrite medium.

Techniques for analyzing electromagnetic scattering by perfectly conducting structures are well established [2-12]. Figure 1.1 gives an example of how a structure with a highly conductive surface (in this

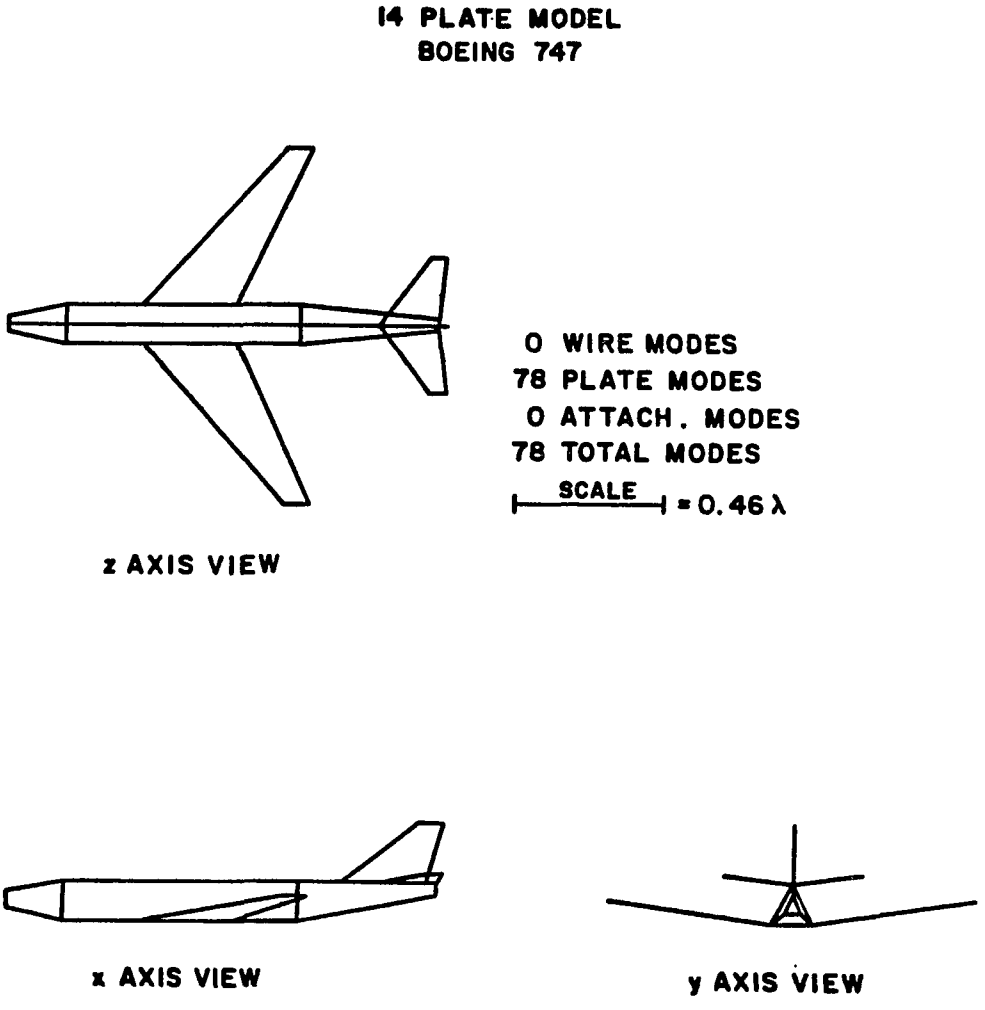

Figure 1.1. A 14 polygonal plate model of a Boeing 747 aircraft.

case, a Boeing 747) can be modelled by a surface patch computer code [13]. Figure 1.1 shows how the surface of a complex structure can be modelled by connecting a series of polygonal plates. One can visualize how a user could model other planes, ships, missiles, etc. In addition, wires can be attached to the surface of the structure, giving the surface path code the versatility to compute a variety of electromagnetic properties, including antenna patterns, mutual coupling between antennas, and radar cross section. To date, one of the limitations of the surface patch code is that if a part of the structure is non-metallic, then the user of the code has only two options: either model the non-metallic parts as perfect conductors, or model them as free space (i.e., ignore the non-metallic parts by not modelling them at all). This dissertation represents the first step in allowing the user to model non-metallic surfaces. In particular, this will be done by analyzing the thin material plate.

Many techniques have been developed for analyzing electromagnetic scattering by non-metallic objects. The classical method of solution uses separation of variables. This method is useful, however, only when the surface of the object coincides with one of the coordinate systems for which the vector Helmholtz equation is separable. Examples include infinite circular cylinders and spheres [14]. Of the many other methods of solving the non-metallic scattering problem (unimoment [15], modal [16] and extended boundry condition [17]), one of the most common involves the formation of integral equations to solve for the equivalent

volume polarization currents. Previously, the polarization current method has been used by Richmond for dielectric cylinders [18], Harrington and Mautz for thin dielectric shells [19], Newman and Tulyathan for wires in the presence of dielectric/ferrite objects [20], and Nyquist, et al., for biological bodies [21]. The polarization current method is particularly useful when treating inhomogeneous media. A second common method of solving a scattering problem is through the use of the surface equivalence principle. The surface equivalence approach has been used by Chang and Harrington for scattering by material bodies [22], and by Wu and Tsai for scattering by layered, lossy dielectric cylinders [23].

Since a goal of this study is to formulate a system of equations that can be easily integrated into existing computer codes that analyze perfectly conducting structures and since the existing computer codes [2-12] are based on the surface equivalence principle, the formulation of the solution presented in this dissertation will also use the surface equivalence approach. The surface equivalence principle applies only to closed surfaces. Thus, in a straight forward application of the surface equivalence principle, the material plate is enclosed in a narrow closed surface. After obtaining the integral equations for the equivalent electric and magnetic surface currents [24], one could solve for the surface currents. However, when the equations are solved by a method such as the method of moments (MM) [25], severe numerical difficulties associated with certain self and

mutual impedances being almost identical would arise [26]. The numerical difficulties can be avoided, however, by taking advantage of certain symmetry properties which allow the integral equations to be rewritten as open surface integral equations. In addition, viewing the material plate as an open surface allows for easier integration into existing solutions for perfectly conducting structures, which are based upon currents flowing on an open surface.

In Chapter II, the theory for the analysis of electromagnetic scattering by a material plate is presented. The result is given in the form of two coupled integral equations. It is shown that as the electrical thickness of the plate vanishes, the solution reduces to a single integral which is identical to the impedance sheet approximation used by Harrington and Mautz [19] and the resistive sheet approximation used by Senior [27].

Chapter III presents a method of moments (MM) solution to the coupled integral equations of Chatper II. Numerous examples are presented to demonstrate the accuracy of the solution for large and small, lossy and lossless, and penetrable and impenetrable plates.

Chapter IV presents the conclusions as well as topics for further study in this area. The appendices evaluate the various fields and mutual impedances that are necessary for a MM solution.

CHAPTER II

THEORY

A solution of electromagnetic scattering by a planar material plate is given in this chapter. In Section A, the material plate is considered as an open surface and, using the reaction integral, four coupled integral equations are derived. In Section B, approximate boundary conditions (abc) are used to obtain two surface impedance relationships. In Section C, the surface impedance relationships derived in Section B replace two of the four coupled integral equations derived in Section A.

A. OPEN SURFACE INTEGRAL EQUATION DEVELOPMENT

Figure 2.1 shows the side view of a material plate with constitutive parameters (μ,ε), and of thickness t, immersed in free space, i.e., a homogeneous medium with constitutive parameters (μ_o,ε_o). The plate is excited by the known impressed currents $(\underline{J}_i,\underline{M}_i)$ which in free space radiate the incident fields $(\underline{E}_i,\underline{H}_i)$, and the unknown fields $(\underline{E},\underline{H})$ in the presence of the plate. Let S denote the surface enclosing the plate. Using the surface equivalence principle [28], Figure 2.1 can be decomposed into the two cases shown in Figure 2.2. In Case A, the

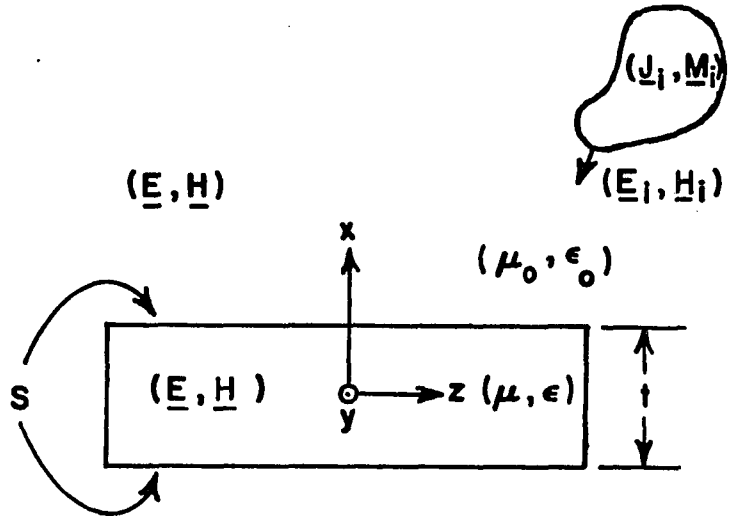

Figure 2.1. Side view of a material plate immersed in free space.

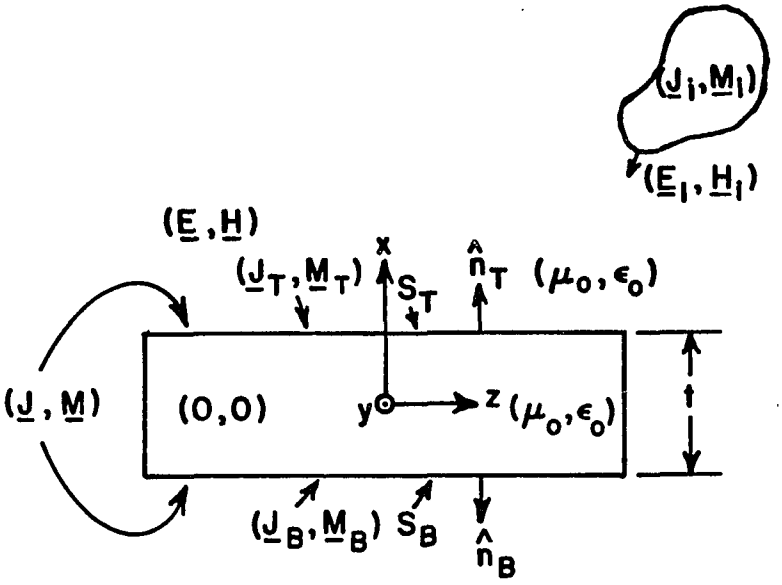

(a) Equivalent solution external to S.

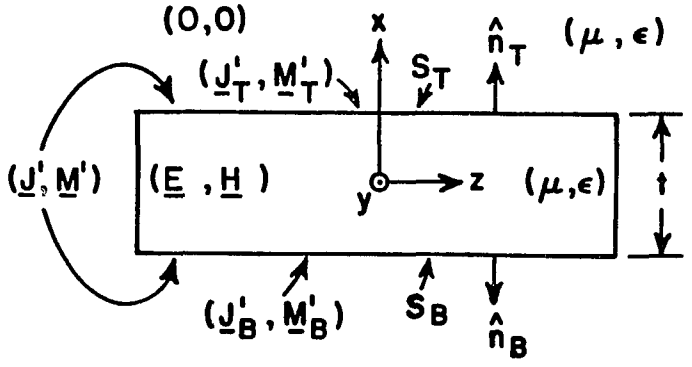

(b) Equivalent solution internal to S.

Figure 2.2. Decomposition of problem in Figure 2.1.

constitutive parameters of all space are (μ_0, ϵ_0), the fields are zero inside the plate, the unknown fields $(\underline{E},\underline{H})$ exist outside the plate, and the surface currents $(\underline{J},\underline{M})$ flow on the surface S. The currents $(\underline{J},\underline{M})$ radiate the scattered fields $(\underline{E}_S,\underline{H}_S)$ in free space. In Case B, the constitutive parameters of all space are (μ,ϵ), the fields are zero outside the plate, the unknown fields $(\underline{E},\underline{H})$ exist inside the plate, and the surface currents $(\underline{J}',\underline{M}') = (-\underline{J},-\underline{M})$ flow on the surface S. Consider that the plates are sufficiently thin so that the surface currents on the sides of the plate can be ignored. Note that use of the surface equivalence principle allows one to evaluate the fields either inside or outside a material body, although one must use the appropriate equivalent geometry (i.e., Case A for fields outside or Case B for fields inside). Further, this statement is not changed by the use of an abc such as surface impedance relationships.

Referring to Figure 2.2, define:

S_T = the top of surface S, i.e., that part of S at $x = t/2$

S_B = the bottom of surface S, i.e., that part of S at $x = -t/2$

$\underline{J}(x,y,z)$ = the electric current flowing on the closed surface S

$\underline{J}_T(y,z)$ = the top electric current, i.e., that part of $\underline{J}$ on S_T

$\underline{J}_B(y,z)$ = the bottom electric current, i.e., that part of $\underline{J}$ on S_B

$\underline{J}_S(y,z)$ = the sum electric current, i.e., a single surface current equal to the vector sum $\underline{J}_T + \underline{J}_B$ and arbitrarily considered to be on S_T

$\underline{J}_D(y,z)$ = the difference electric current, i.e., a single surface current equal to the vector difference $\underline{J}_T - \underline{J}_B$ and arbitrarily considered to be on S_T

$\underline{M}(x,y,z)$ = the magnetic current flowing on the closed surface S

$\underline{M}_T(y,z)$ = the top magnetic current, i.e., that part of $\underline{M}$ on S_T

$\underline{M}_B(y,z)$ = the bottom magnetic current, i.e., that part of $\underline{M}$ on S_B

$\underline{M}_S(y,z)$ = the sum magnetic current, i.e., $\underline{M}_T + \underline{M}_B$ and arbitrarily considered to be on S_T

$\underline{M}_D(y,z)$ = the difference magnetic current, i.e., $\underline{M}_T - \underline{M}_B$ and arbitrarily considered to be on S_T.

Now consider the problem of Figure 2.2a. Since a null field exists interior to S, there will be zero reaction between the currents $(\underline{J},\underline{M})$ and $(\underline{J}_i,\underline{M}_i)$, and a test source interior to S. If the test source is electric with current density $\underline{J}_t$, this leads to the electric reaction integral equation (ERIE)

$$- \langle \underline{J}_t, (\underline{J},\underline{M}) \rangle = V^J \tag{2.1}$$

where

$$V^J = \langle \underline{J}_t, (\underline{J}_i,\underline{M}_i) \rangle \quad . \tag{2.2}$$

By definition [29], the reaction between sources a and b is

$$\langle a,b \rangle = \iint_b (\underline{E}_a \cdot \underline{J}_b - \underline{H}_a \cdot \underline{M}_b)\, ds = \langle b,a \rangle \tag{2.3}$$

where the integral is over the region occupied by the source b.

Figure 2.3 shows the side view of the plate with an electric test source $\underline{J}_t$ in the interior. $\underline{J}_t$ is considered to be a surface current in the yz plane, and its fields in free space will be denoted $(\underline{E}^J_t, \underline{H}^J_t)$. The plate currents $(\underline{J},\underline{M})$ are explicitly shown as $(\underline{J}_T,\underline{M}_T)$ on S_T and $(\underline{J}_B,\underline{M}_B)$ on S_B. Using the linearity of the reaction operator, Equation (2.1) becomes

$$- \langle \underline{J}_t, (\underline{J}_T, \underline{M}_T) \rangle - \langle \underline{J}_t, (\underline{J}_B, \underline{M}_B) \rangle = V^J \quad , \tag{2.4}$$

or

$$- \iint_{S_T} (\underline{E}^J_t \cdot \underline{J}_T - \underline{H}^J_t \cdot \underline{M}_T)\, ds - \iint_{S_B} (\underline{E}^J_t \cdot \underline{J}_B - \underline{H}^J_t \cdot \underline{M}_B) ds = V^J \quad . \tag{2.5}$$

Since the tangential magnetic field of $\underline{J}_t$ is discontinuous by $\underline{J}_t$ across $\underline{J}_t$, for a thin plate

$$\hat{n}_T \times [\underline{H}^J_t(S_T) - \underline{H}^J_t(S_B)] \underset{\ell im\ t \to 0}{=} \underline{J}_t \quad . \tag{2.6}$$

Also by symmetry, $\hat{n}_T \times \underline{H}^J_t(S_T) = -\hat{n}_T \times \underline{H}^J_t(S_B)$. Hence it follows from Equation (2.6) that

$$\hat{n}_T \times \underline{H}^J_t(S_T) = -\hat{n}_T \times \underline{H}^J_t(S_B) \underset{\ell im\ t \to 0}{=} \underline{J}_t/2 \quad . \tag{2.7}$$

In addition, since the tangential electric field of $\underline{J}_t$ is continuous across $\underline{J}_t$

$$\underline{E}_t^J(S_T) \times \hat{n}_T = \underline{E}_t^J(S_B) \times \hat{n}_T \quad . \tag{2.8}$$

Using the symmetry relations of Equations (2.7) and (2.8) the bottom currents $(\underline{J}_B, \underline{M}_B)$ are moved from S_B to S_T, and Equation (2.5) becomes

$$- \iint_{S_T} [\underline{E}_t^J \cdot (\underline{J}_T + \underline{J}_B) - \underline{H}_t^J \cdot (\underline{M}_T - \underline{M}_B)] \, ds = V^J \quad , \quad \text{or} \tag{2.9}$$

$$- \langle \underline{J}_t, (\underline{J}_S, \underline{M}_D) \rangle = V^J . \tag{2.10}$$

Note that Equation (2.10) applies on the open surface S_T.

Next consider the case where the test source in Equation (2.3) is the magnetic current $\underline{M}_t$. This leads to the magnetic reaction integral equation (MRIE)

$$- \langle \underline{M}_t, (\underline{J}, \underline{M}) \rangle = V^M \tag{2.11}$$

where

$$V^M = \langle \underline{M}_t, (\underline{J}_i, \underline{M}_i) \rangle \quad . \tag{2.12}$$

Figure 2.3 shows the side view of the plate with a magnetic test source $\underline{M}_t$ in the interior. $\underline{M}_t$ is considered to be a surface current in the yz plane, and its fields in free space will be denoted $(\underline{E}_t^M, \underline{H}_t^M)$. Again, using the linearity of the reaction operator, Equation (2.11) becomes

$$- \langle \underline{M}_t, (\underline{J}_T, \underline{M}_T) \rangle - \langle \underline{M}_t, (\underline{J}_B, \underline{M}_B) \rangle = V^M \quad , \tag{2.13}$$

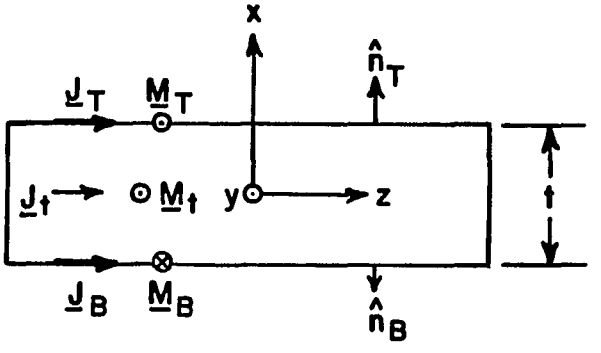

Figure 2.3. Side view of a material plate with an electric test source, $\underline{J}_t$, and a magnetic test source, $\underline{M}_t$, in the interior.

or

$$- \iint_{S_T} (\underline{E}_t^M \cdot \underline{J}_T - \underline{H}_t^M \cdot \underline{M}_T)ds - \iint_{S_B} (\underline{E}_t^M \cdot \underline{J}_B - \underline{H}_t^M \cdot \underline{M}_B)ds = V^M \ . \tag{2.14}$$

Since the tangential electric field of $\underline{M}_t$ is discontinuous by $\underline{M}_t$ as one crosses $\underline{M}_t$, for a thin plate

$$[\underline{E}_t^M(S_T) - \underline{E}_t^M(S_B)] \times \hat{n}_T \underset{\ell im\ t\to 0}{=} \underline{M}_t \ . \tag{2.15}$$

Also by symmetry, $\underline{E}_t^M(S_T) \times \hat{n}_T = -\underline{E}_t^M(S_B) \times \hat{n}_T$. Hence it follows from Equation (2.15) that

$$\underline{E}_t^M(S_T) \times \hat{n}_T = -\underline{E}_t^M(S_B) \times \hat{n}_T \underset{\ell im\ t\to 0}{=} \underline{M}_t/2 \ . \tag{2.16}$$

In addition, since the tangential magnetic field of $\underline{M}_t$ is continuous across $\underline{M}_t$

$$\hat{n}_T \times \underline{H}_t^M(S_T) = \hat{n}_T \times \underline{H}_t^M(S_B) \ . \tag{2.17}$$

Using the symmetry relations of Equations (2.16) and (2.17), $(\underline{J}_B, \underline{M}_B)$ are again moved from S_B to S_T, and Equation (2.14) becomes

$$-\iint_{S_T} [\underline{E}_t^M \cdot (\underline{J}_T - \underline{J}_B) - \underline{H}_t^M \cdot (\underline{M}_T + \underline{M}_B)] \, ds = V^M \ , \tag{2.18}$$

or

$$- < \underline{M}_t, (\underline{J}_D, \underline{M}_S) > = V_M \quad , \tag{2.19}$$

valid on the open surface S_T.

Equations (2.10) and (2.19) constitute two of the four equations needed to solve for the four unknowns, $(\underline{J}_S, \underline{M}_S)$ and $(\underline{J}_D, \underline{M}_D)$. In obtaining these equations, the plate thickness was not required to go to zero. The thickness does have to be sufficiently small that the side currents can be ignored. To obtain the remaining two equations, the zero reaction concept with test sources outside S is applied to the equivalent problem of Figure 2.2b. An arbitrary test source $(\underline{J}_t, \underline{M}_t)$ exterior to S in Figure 2.2b has zero reaction with the currents $(\underline{J}', \underline{M}') = (-\underline{J}, -\underline{M})$, or

$$<(\underline{J}_t, \underline{M}_t), (\underline{J}, \underline{M})> = 0. \tag{2.20}$$

Explicitly showing the integrations over the top and bottom surfaces, Equation (2.20) becomes

$$\iint_{S_T} (\underline{E}_t \cdot \underline{J}_T - \underline{H}_t \cdot \underline{M}_T) ds + \iint_{S_B} (\underline{E}_t \cdot \underline{J}_B - \underline{H}_t \cdot \underline{M}_B) ds = 0 \quad , \tag{2.21}$$

where $(\underline{E}_t, \underline{H}_t)$ are the fields of $(\underline{J}_t, \underline{M}_t)$ in the homogeneous medium (μ, ε). In practice, two independent equations can be obtained from Equation (2.20) by first placing $(\underline{J}_t, \underline{M}_t)$ in the plane $x = (t + \Delta t)/2$ and then in the plane $x = -(t+\Delta t)/2$ where Δt is a small positive value. Thus, Equations (2.10), (2.19), and (2.20) twice constitute four coupled

integral equations which could, in principle, be solved for $(\underline{J}_S, \underline{M}_S)$ and $(\underline{J}_D, \underline{M}_D)$. In order to properly account for plate thickness, one should convert the sum and difference currents to top and bottom currents prior to computing the scattered fields (interior or exterior to the plate). However, for thin plates and exterior field points whose radial distance from the plate is large in comparison to plate thickness, one may compute the scattered fields from $(\underline{J}_S, \underline{M}_S)$ only.

B. APPROXIMATE IMPEDANCE BOUNDARY CONDITION

In this section the surface impedance relationships for a penetrable dielectric/ferrite plane sheet or slab and an impenetrable perfectly conducting ground plane coated on one or both sides by a dielectric/ferrite material will be obtained. This will be done by considering the simple one dimensional problem of a plane wave normally incident upon a dielectric/ferrite slab. Although the solution to this problem in terms of plane wave reflections appears in many texts on electromagnetic theory [30], the solution will be investigated using the surface equivalence principle and the reaction integral equations obtained in the previous section. For the case of the slab, Equation (2.20) has simple solutions from which we can deduce relationships between the equivalent electric and magnetic surface currents, i.e., the slab surface impedance relationships. In the next section, the approximation that these relationships (which are exact for

the slab) apply also to the finite or three dimensional material plate, will be employed. This will eliminate two of the four integral equations for the material plate.

Figure 2.4 shows a plane wave of the form

$$\underline{E}_i = \hat{z}\, E_0\, e^{\gamma_0 x} \quad , \tag{2.22a}$$

$$\underline{H}_i = \hat{y}\, E_0\, e^{\gamma_0 x} / \eta_0 \quad , \tag{2.22b}$$

where $\gamma_0 = j\omega\sqrt{\mu_0\varepsilon_0}$ and $\eta_0 = \sqrt{\frac{\mu_0}{\varepsilon_0}}$, incident upon a slab of thickness t and with parameters (μ,ε). The illuminated surface of the slab at $x = t/2$ will be referred to as S_T, the top surface. The surface at $x = -t/2$ will be referred to as S_B, the bottom surface. In direct analogy to Figure 2.2, the equivalent currents will be constant sheets denoted $(J_T\hat{z}, M_T\hat{y})$ on S_T and $(J_B\hat{z}, -M_B\hat{y})$ on S_B. Referring to Figure 2.4 and Equation (2.20), there will be zero reaction between a constant sheet current test source located outside the slab and the equivalent currents (J_T, M_T) and (J_B, M_B). If the test source is given by the electric current

$$\underline{J}_t = -2\hat{z} \quad , \tag{2.23}$$

and is located in the plane $x = x_t$ $(|x_t| > t/2)$ then its fields in the medium (μ,ε) are

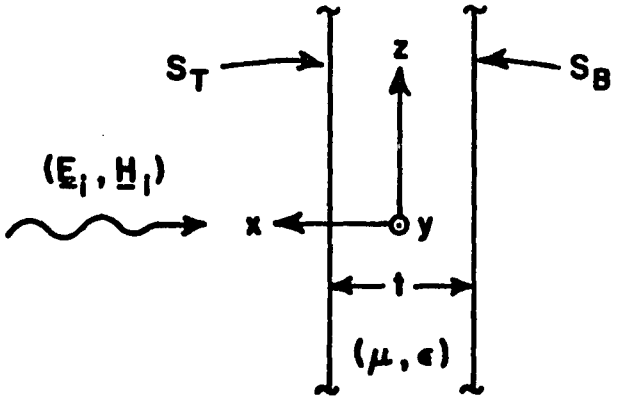

Figure 2.4. Side view of a material slab immersed in free space.

$$\underline{E}_t = \hat{z}\, \eta\, e^{-\gamma|x-x_t|} \quad , \tag{2.24a}$$

$$\underline{H}_t = -\hat{y}\, \mathrm{sgn}\,(x-x_t)\, e^{-\gamma|x-x_t|} \quad , \tag{2.24b}$$

where $\eta = \sqrt{\frac{\mu}{\varepsilon}}$, $\gamma = j\omega\sqrt{\mu\varepsilon}$, and sgn(x) = 1 if x > 0 and -1 if x < 0.

Inserting Equations (2.23) and (2.24) into Equation (2.21) yields

$$\left(\eta J_T + \mathrm{sgn}(t/2-x_t) M_T\right) e^{-\gamma|t/2-x_t|} \iint_{S_T} ds$$

$$+ \left(\eta J_B - \mathrm{sgn}(-t/2-x_t) M_B\right) e^{-\gamma|-t/2-x_t|} \iint_{S_B} ds = 0 \tag{2.25}$$

or,

$$J_T \eta e^{-\gamma t/2} + J_B \eta e^{\gamma t/2} + M_T e^{-\gamma t/2} - M_B e^{\gamma t/2} = 0 \text{ for } x_t < -t/2 \ , \tag{2.26a}$$

$$J_T \eta e^{\gamma t/2} + J_B \eta e^{-\gamma t/2} - M_T e^{\gamma t/2} + M_B e^{-\gamma t/2} = 0 \text{ for } x_t > t/2 \ . \tag{2.26b}$$

Solving Equations (2.26) for M_T and M_B yields

$$M_T = Z_{TT} J_T + Z_{TB} J_B \quad , \tag{2.27a}$$

$$M_B = Z_{BT} J_T + Z_{BB} J_B \quad , \tag{2.27b}$$

where

$$Z_{TT} = Z_{BB} = \eta/\tanh\gamma t \quad , \tag{2.28a}$$

$$Z_{TB} = Z_{BT} = \eta/\sinh\gamma t \quad . \tag{2.28b}$$

These impedances are equal to the two port impedance parameters of the transmission line of length t, characteristic impedance η, and propagation constant γ, shown in Figure 2.5.

If the slab had been impenetrable, such as the perfectly conducting ground plane coated on one or both sides by a dielectric/ferrite slab of Figure 2.6, then the two port impedances would be those of the short-circuited transmission line model of Figure 2.7. In this case [31] $Z_{TB} = Z_{BT} = 0$, and

$$Z_{TT} = \eta_1 \tanh\gamma_1 t_1 \quad , \tag{2.29a}$$

$$Z_{BB} = \eta_2 \tanh\gamma_2 t_2 \quad . \tag{2.29b}$$

C. SURFACE IMPEDANCE APPROXIMATION

In the last section, two impedance boundary relationships (Equations (2.27)) for a one dimensional dielectric/ferrite slab were obtained. In this section, Equations (2.27) are used as an approximation for Equation (2.20). For a one dimensional slab at normal incidence these relationships are exact. For a three dimensional material plate they are not exact since:

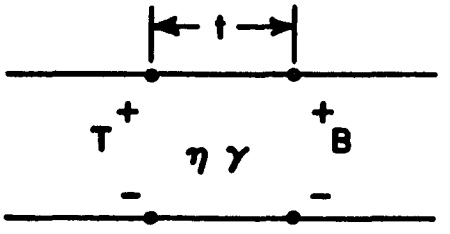

Figure 2.5. Transmission line model equivalent to Figure 2.4.

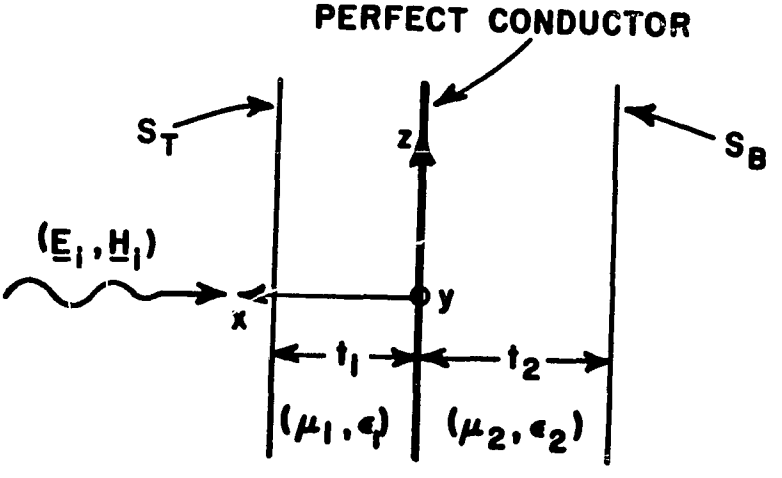

Figure 2.6. Side view of a coated, perfectly conducting sheet immersed in free space.

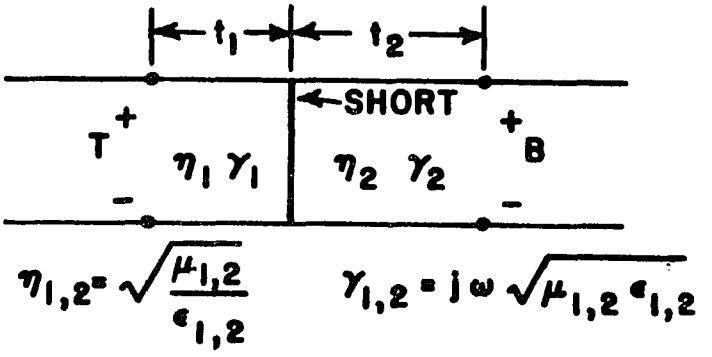

Figure 2.7. Transmission line model equivalent to Figure 2.6.

(1) the incident wave may not have normal incidence,

(2) the edges and corners of the plate will modify the relationships.

Despite this, the one dimensional slab surface impedance relationships for the three dimensional material plate will be used. This is an application of what Senior [32] termed an approximate boundary condition (abc). As pointed out by Senior, there usually is no rigorous justification for the use of an abc. The justification is in its usefulness in predicting results obtained by measurements or by more rigorous techniques. Of course, the motivation for their use as compared to more rigorous techniques is that they simplify the analysis. Writing Equations (2.27) in terms of sum and difference currents gives

$$\underline{M}_S = Z_{SS}\underline{J}_S \times \hat{n}_T + Z_{SD}\underline{J}_D \times \hat{n}_T \quad , \tag{2.30a}$$

$$\underline{M}_D = Z_{DS}\underline{J}_S \times \hat{n}_T + Z_{DD}\underline{J}_D \times \hat{n}_T \quad . \tag{2.30b}$$

where

$$Z_{SS} = (Z_{TT} + Z_{TB} - Z_{BT} - Z_{BB})/2 \quad , \tag{2.31a}$$

$$Z_{SD} = (Z_{TT} - Z_{TB} - Z_{BT} + Z_{BB})/2 \quad , \tag{2.31b}$$

$$Z_{DS} = (Z_{TT} + Z_{TB} + Z_{BT} + Z_{BB})/2 \quad , \tag{2.31c}$$

$$Z_{DD} = (Z_{TT} - Z_{TB} + Z_{BT} - Z_{BB})/2 \quad . \tag{2.31d}$$

Combining Equations (2.10), (2.19), and (2.30) yields

$$- \langle \underline{J}_t, (\underline{J}_S, \underline{M}_D) \rangle = - \langle \underline{J}_t, (\underline{J}_S, Z_{DS}\underline{J}_S \times \hat{n}_T + Z_{DD}\underline{J}_D \times \hat{n}_T) \rangle = V^J \quad , \tag{2.32a}$$

$$- \langle \underline{M}_t, (\underline{J}_D, \underline{M}_S) \rangle = - \langle \underline{M}_t, (\underline{J}_D, Z_{SS}\underline{J}_S \times \hat{n}_T + Z_{SD}\underline{J}_D \times \hat{n}_T) \rangle = V^M \quad . \tag{2.32b}$$

Equations (2.32) represent two coupled integral equations on the open surface S_T which can be solved for the electric currents $\underline{J}_S$ and $\underline{J}_D$. Having solved for $\underline{J}_S$ and $\underline{J}_D$, the magnetic currents $\underline{M}_S$ and $\underline{M}_D$ can be found from Equations (2.30). Recall that the $Z_{DS}\underline{J}_S \times \hat{n}_T + Z_{DD}\underline{J}_D \times \hat{n}_T$ and $Z_{SS}\underline{J}_S \times \hat{n}_T + Z_{SD}\underline{J}_D \times \hat{n}_T$ terms in Equation (2.32) are not electric currents, but rather are the magnetic currents, $\underline{M}_D$ and $\underline{M}_S$, respectively.

In the remaining part of this section, Equations (2.32) are examined for various special cases.

CASE 1 - PERFECTLY CONDUCTING PLATES

If the plate is a perfect conductor, then $Z_{SS} = Z_{DD} = Z_{DS} = Z_{SD} = 0$ and Equations (2.32) reduce to

$$-\langle \underline{J}_t, (\underline{J}_S, 0) \rangle = V^J \quad , \tag{2.33a}$$

$$-\langle \underline{M}_t, (\underline{J}_D, 0) \rangle = V^M \quad . \tag{2.33b}$$

Equation (2.33a) or a similar equation is a widely published and used expression [8-11] for the solution of scattered fields by perfectly conducting plates. However, when coupled with Equation (2.33b), one can solve for currents on both sides of a perfectly conducting plate [33].

CASE 2 - UNIFORM MATERIAL PLATE

If the plate is homogeneous then from Equations (2.28) and (2.31), $Z_{SS} = Z_{DD} = 0$ and

$$Z_{SD} = Z_{TT} - Z_{TB} = \eta(\cosh\gamma t - 1)/\sinh\gamma t \quad , \tag{2.34a}$$

$$Z_{DS} = Z_{TT} + Z_{TB} = \eta(\cosh\gamma t + 1)/\sinh\gamma t \quad . \tag{2.34b}$$

In this case, Equations (2.32) reduce to

$$- \langle \underline{J}_t, (\underline{J}_S, \underline{M}_D) \rangle = -\langle J_t, (\underline{J}_S, Z_{DS}\underline{J}_S \times n_T) \rangle = V^J \quad , \tag{2.35a}$$

$$- \langle \underline{M}_t, (\underline{J}_D, \underline{M}_S) \rangle = -\langle \underline{M}_t, (\underline{J}_D, Z_{SD}\underline{J}_D \times \hat{n}_T) \rangle = V^M \quad . \tag{2.35b}$$

An important point is that the equations uncouple for this case. However, note that both equations must be solved to find $(\underline{J}_S, \underline{M}_S)$ which radiate the far-zone scattered field. In general, for any symmetric slab (i.e., $Z_{TT}=Z_{BB}$ and $Z_{TB}=Z_{BT}$) the equations uncouple.

CASE 3 - THIN UNIFORM MATERIAL PLATE

Now consider Equation (2.35a) in the limit as the thickness γt goes to zero. As noted earlier, to find the scattered field, both $\underline{J}_S$ and $\underline{M}_S$ must be solved. However, in this case, from Equations (2.30a) and (2.34)

$$\lim_{\gamma t \to 0} \underline{M}_S = Z_{SD}\underline{J}_D \times \hat{n}_T = \lim_{\gamma t \to 0} \eta \frac{\cosh \gamma t - 1}{\sinh \gamma t} \underline{J}_D \times \hat{n}_T = 0 \quad . \tag{2.36}$$

Thus, to solve for the scattered field of a uniform material plate as $\gamma t \to 0$, only $\underline{J}_S$ in Equation (2.35a) must be solved. By reciprocity, Equation (2.35a) can be written as

$$- \iint_t \underline{J}_t \cdot (\underline{E}(\underline{J}_S) + \underline{E}(\underline{M}_D) + \underline{E}_i)\, ds = 0 \quad , \tag{2.37}$$

where $\underline{E}(\underline{J}_S)$ and $\underline{E}(\underline{M}_D)$ are the free-space electric fields of $\underline{J}_S$ and $\underline{M}_D = Z_{DS}\, \underline{J}_S \times \hat{n}_T$, respectively, and the integral is over the surface of the arbitrary electric test source $\underline{J}_t$. Note that $\underline{J}_t$ is located in the interior of the closed surface S and is tangential to the broad surfaces of S.

Since Equation (2.37) must apply for an arbitrary $\underline{J}_t$, it is clear that

$$\underline{E}_{tan}(\underline{J}_S) + \underline{E}_{tan}(\underline{M}_D) = - \underline{E}_{i\ tan} \text{ interior to S.} \tag{2.38}$$

As $\gamma t \to 0$, the tangential electric field of $\underline{M}_D$ will be essentially (see Equation (2.16))

$$E_{tan}(\underline{M}_D) = - \hat{n}_T \times \underline{M}_D/2 \quad . \tag{2.39}$$

Also from Equation (2.34b),

$$\lim_{\gamma t \to o} Z_{DS} = \frac{2\eta}{\gamma t} \quad . \tag{2.40}$$

Combining Equations (2.30b) and (2.38)-(2.40) gives

$$-\underline{E}_{tan}(\underline{J}_S) + \frac{\eta}{\gamma t}\underline{J}_S = \underline{E}_{i\ tan} \quad . \tag{2.41}$$

Equation (2.41) gives the current on a surface of sheet impedance $\eta/\gamma t$. It is equivalent to that used by Harrington to study thin dielectric shells [19] and by Senior to study resistive strips [27]. Note that when treating impedance sheets, one simply adds the term $\frac{\eta}{\gamma t}\underline{J}_S$ to the equation for perfectly conducting surfaces. In a MM solution of Equation (2.41) this would result in an impedance matrix of the form [Z] + [ΔZ] where [Z] is the impedance matrix for the perfectly conducting surface, and a typical term of [ΔZ] would be

$$\Delta Z_{mn} = \frac{\eta}{\gamma t}\iint \underline{J}_m \cdot \underline{G}_n \ ds \quad . \tag{2.42}$$

Here $\underline{J}_m$ represents the m^{th} current expansion mode and $\underline{G}_n$ the n^{th} test mode or weighting function. Equation (2.42) can be evaluated in closed form for any of the usual choices for the modes. This permits the thin symmetric slab to be treated as a very simple modification of the perfect conductor. Note that $\Delta Z_{mn} = 0$ unless modes $\underline{J}_m$ and $\underline{G}_n$ overlap. Also, for extremely small γt, ΔZ_{mn} will be large, and this will result in small $\underline{J}_S$.

CASE 4 - COATED CONDUCTING PLATE

If the plate is a perfect conductor coated on one or both sides by a dielectric/ferrite, then from Equations (2.29) and (2.31)

$$Z_{SS} = Z_{DD} = (\eta_1 \tanh\gamma_1 t_1 - \eta_2 \tanh\gamma_2 t_2)/2 \quad , \tag{2.43a}$$

$$Z_{SD} = Z_{DS} = (\eta_1 \tanh\gamma_1 t_1 + \eta_2 \tanh\gamma_2 t_2)/2 \quad , \tag{2.43b}$$

and Equations (2.32) reduce to the coupled equations

$$- \langle \underline{J}_t, (\underline{J}_S, \underline{M}_D) \rangle = -\langle \underline{J}_t, (\underline{J}_S, Z_{SD}\underline{J}_S \times \hat{n}_T + Z_{SS}\underline{J}_D \times \hat{n}_T) \rangle = V^J \quad , \tag{2.44a}$$

$$- \langle \underline{M}_t, (\underline{J}_D, \underline{M}_S) \rangle = -\langle \underline{M}_t, (\underline{J}_D, Z_{SS}\underline{J}_S \times \hat{n}_T + Z_{SD}\underline{J}_D \times \hat{n}_T) \rangle = V^M \quad . \tag{2.44b}$$

CHAPTER III

SOLUTION OF INTEGRAL EQUATIONS

In Section A of this chapter, a moment method solution of the coupled integral Equations (2.32) is presented. In Section B, numerical results of the moment method solution are given. Since the abc or surface impedance results of Equations (2.30) do not rigorously apply to three dimensional plates, numerical results of several examples are presented. The justification of the use of the abc is the accuracy of the numerical results.

A. MOMENT METHOD SOLUTION

The current distributions on the material plates can be found by solving the integral equations of the previous section by the numerical techniques known as the method of moments (MM) [25]. Here the MM solution to Equations (2.32), which represents the most general case rather than one of the special cases which follow, is presented. The solution is similar to that for perfectly conducting surfaces [4,11,12].

The first step in the MM solution is to expand the unknown currents, $\underline{J}_S$ and $\underline{J}_D$, in a finite set of N basis functions:

$$\underline{J}_S = \sum_{n=1}^{N} I_{Sn}\, \underline{F}_n \quad , \tag{3.1a}$$

$$\underline{J}_D = \sum_{n=1}^{N} I_{Dn}\, \underline{F}_n \quad , \tag{3.1b}$$

where $\underline{F}_n$ is a normalized expansion function and I_{Sn} and I_{Dn} are complex constants. Then using the abc's of Equations (2.30), $\underline{M}_S$ and $\underline{M}_D$ are the dependent unknowns

$$\underline{M}_S = \sum_{n=1}^{N} (Z_{SS}\, I_{Sn} + Z_{SD}\, I_{Dn})\, \underline{F}_n \times \hat{n}_T \quad , \tag{3.2a}$$

$$\underline{M}_D = \sum_{n=1}^{N} (Z_{DS}\, I_{Sn} + Z_{DD}\, I_{Dn})\, \underline{F}_n \times \hat{n}_T \quad . \tag{3.2b}$$

Refering to Figure 2.3 and choosing our test modes identical to the expansion modes (except that they are in the yz plane), Equations (2.32) reduce to the set of 2N simultaneous linear equations written in block matrix form as

$$\begin{bmatrix} [Z^{EE}] + Z_{DS}\,[Z^{EM}] & [Z^{EM}] + Z_{DD}\,[Z^{EM}] \\ [Z^{ME}] + Z_{SS}\,[Z^{MM}] & [Z^{ME}] + Z_{SD}\,[Z^{MM}] \end{bmatrix} \begin{bmatrix} I_S \\ I_D \end{bmatrix} = \begin{bmatrix} V^J \\ V^M \end{bmatrix} \quad , \tag{3.3}$$

where

$$Z_{mn}^{EE} = - \iint_n \underline{E}_m^J \cdot \underline{F}_n \, ds \quad , \tag{3.4a}$$

$$Z_{mn}^{EM} = \iint_n \underline{H}_m^J \cdot (\underline{F}_n \times \hat{n}_T) \, ds \quad , \tag{3.4b}$$

$$Z_{mn}^{ME} = - \iint_n \underline{E}_m^M \cdot \underline{F}_n \, ds \quad , \tag{3.4c}$$

$$Z_{mn}^{MM} = \iint_n \underline{H}_m^M \cdot (\underline{F}_n \times \hat{n}_T) \, ds \quad , \tag{3.4d}$$

$$V_m^J = \iiint_v (\underline{J}_i \cdot \underline{E}_m^J - \underline{M}_i \cdot \underline{H}_m^J) \, dv \quad , \tag{3.5a}$$

$$V_m^M = \iiint_v (\underline{J}_i \cdot \underline{E}_m^M - \underline{M}_i \cdot \underline{H}_m^M) \, dv \quad . \tag{3.5b}$$

The integrations in Equations (3.4) are over the surface of the n^{th} expansion mode located on S_T. $(\underline{E}_m^J, \underline{H}_m^J)$ and $(\underline{E}_m^M, \underline{H}_m^M)$ are the free space fields of the m^{th} electric and magnetic test modes, respectively. For simplicity, in the numerical evaluation of Equations (3.4), the plate is considered to have infintesimal thickness. Thus, material plates of finite thickness are modeled by infinitesimally thin plates with some surface impedance. The only place that the actual plate thickness enters the present computation is in the evaluation of the surface impedance relationships. The matrices $[Z^{EE}]$ and $[Z^{MM}]$ are symmetric since the test and expansion modes used in the computation of their elements are identical (except for a position shift of $t/2$, $t \to 0$). In general, the matrices $[Z^{EM}]$, $[Z^{ME}]$ are not symmetric because their test

and expansion modes are not identical. For example, in the computation of the element Z_{mn}^{EM}, the m^{th} mode is a test mode with electric current density $\underline{F}_m$, while the n^{th} mode is an expansion mode with magnetic current density $\underline{F}_n \times \hat{n}_T$. Details of the evaluation of the impedance elements Z_{mn}^{EE}, Z_{mn}^{EM}, Z_{mn}^{ME} and Z_{mn}^{MM} are given in Appendix B.

A typical test or expansion surface-patch mode is shown in Figure 3.1. A surface patch dipole mode consists of two speed-of-light sinusoidal surface patch monopoles. The current on the surface-patch dipole mode of Figure 3.1 is given by

$$\underline{F} = \hat{z}\, P_1 \frac{\gamma_0 \sinh\gamma_0(z-z_2)\cosh\gamma_0 x}{2\sinh\gamma_0(z_1-z_2)\sinh\gamma_0 w} + \hat{z}\, P_2 \frac{\gamma_0 \sinh\gamma_0(z_3-z)\cosh\gamma_0 x}{2\sinh\gamma_0(z_3-z_1)\sinh\gamma_0 w}\ , \tag{3.6}$$

where P_1 and P_2 represent pulse functions with unit value on monopole 1 and 2, respectively, and zero elsewhere, and $\gamma_0 = j\omega\sqrt{\mu_0\varepsilon_0}$. The dipole has endpoints at z_2 and z_3 and terminals at z_1.

A typical rectangular plate is shown in Figure 3.2. Two orthgonal and overlapping sets of surface-patch modes cover the surface of the plate forming a two-dimensional vector surface density which could be used to represent $\underline{J}_S$, $\underline{J}_D$, $\underline{M}_S$, or $\underline{M}_D$. To insure the continuity of current, the normal components of $\underline{J}_S$ and $\underline{M}_D$ must vanish at a plate edge, however, the normal components of $\underline{J}_D$ and $\underline{M}_S$ do not. Thus, a series of edge modes consisting of a single monopole with terminals at the plate edge is included. This allows for a non-zero normal component of

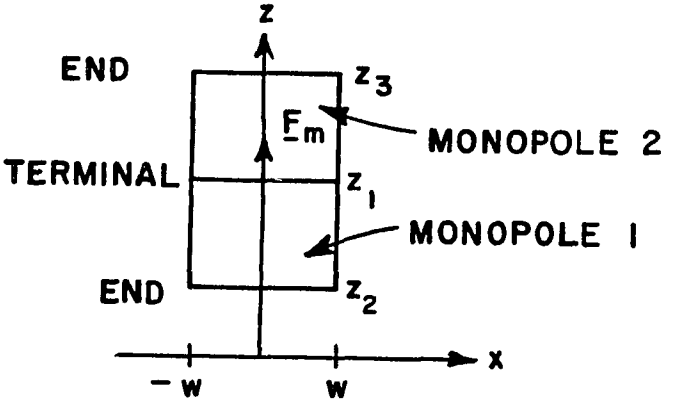

Figure 3.1. Piece-wise sinusoidal surface patch dipole mode.

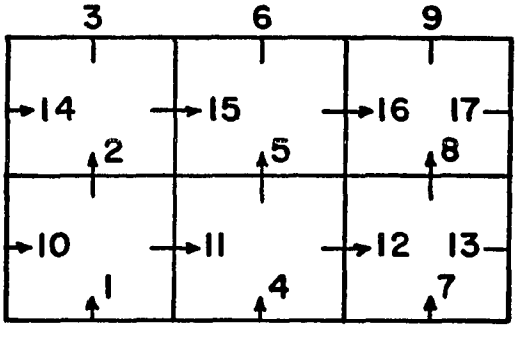

Figure 3.2. Surface patch dipole mode layout for a flat plate.

current at the plate edge. The plate in Figure 3.2 is made up of ten monopole edge modes and seven dipole interior modes. The monopole edge modes will be identically zero for $\underline{J}_S$ and $\underline{M}_D$, but not for $\underline{J}_D$ and $\underline{M}_S$.

B. NUMERICAL RESULTS

In this section, numerical results using the moment method solution outlined in the previous section will be presented. Although most of the data will be for scattering by a material plate, the solution of Equations (2.33), which permit the computation of the currents on the top and bottom of a perfectly conducting plate, will be investigated. Data will be shown for the magnitude of the currents induced on a square, perfectly conducting plate by a normally incident plane wave. This is accomplished by applying the moment method solution to Equations (2.33).

Figure 3.3 shows an L by L square plate in the yz plane. It is excited by a plane wave with a $\hat{z}$ polarized electric field incident from the positive x axis and magnetic field intensity $\underline{H}_i$. Currents will be shown along the line $y = 0$ and $0 < z < L$. Currents will be normalized by $2|H_i|$, i.e., the magnitude of the physical optic currents. The sum $\underline{H}_i$ and difference currents are plotted on one axis, and the top (illuminated) and bottom currents on another axis. Figures 3.4 - 3.8 show currents for $L = 0.125\lambda$, 0.25λ, 0.5λ, 1.0λ, and 2.0λ, respectively. Note the following from these figures:

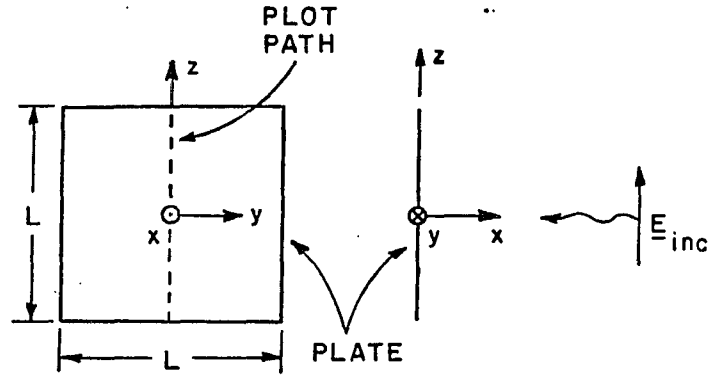

Figure 3.3. Plane wave normally incident on a square, perfectly conducting plate.

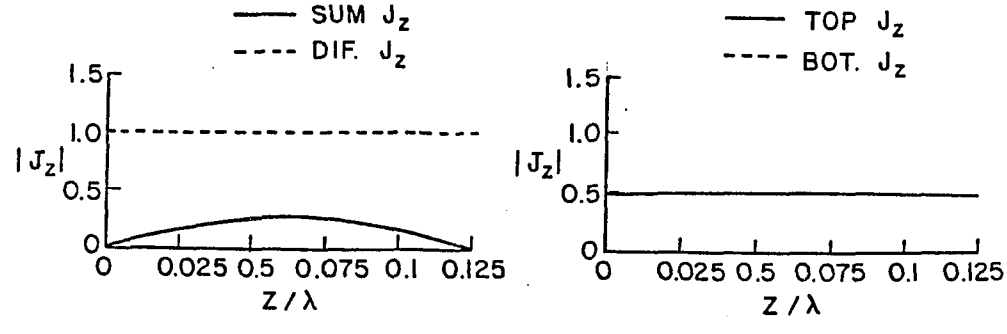

Figure 3.4. Currents on a 0.125λ square plate normalized to $2|\underline{H}_i|$.

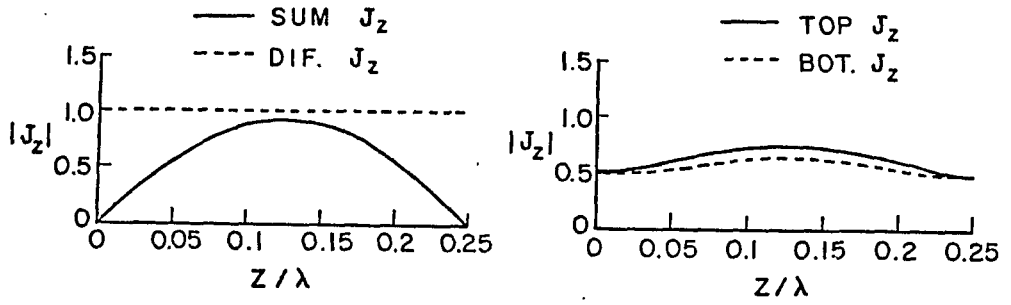

Figure 3.5. Currents on a 0.25λ square plate normalized to $2|\underline{H}_i|$.

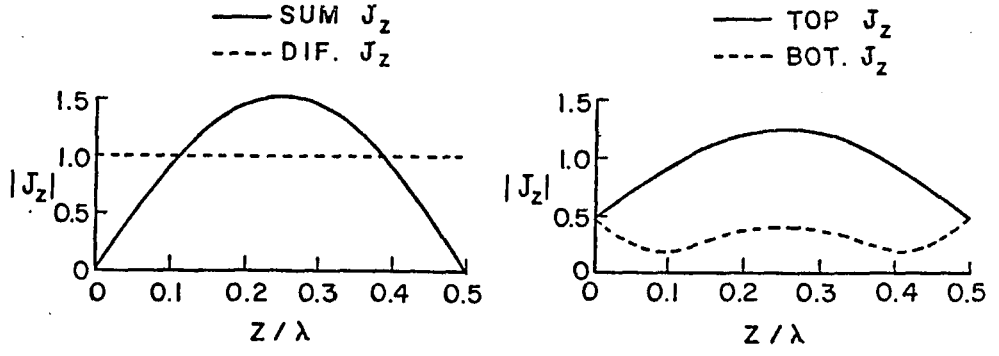

Figure 3.6. Currents on a 0.50λ square plate normalized to $2|\underline{H}_i|$.

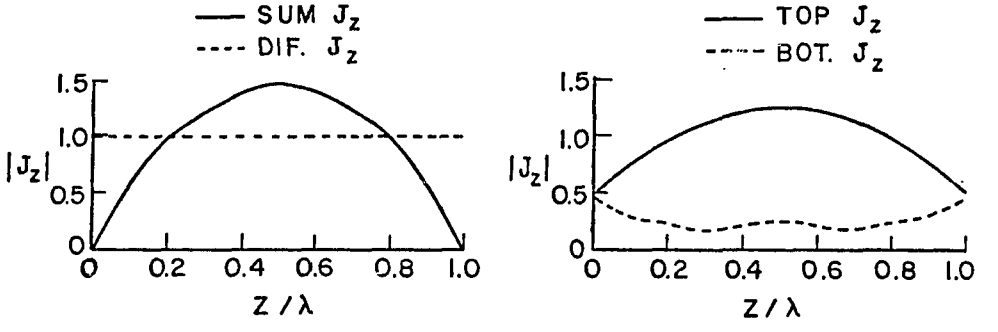

Figure 3.7. Currents on a 1.0λ square plate normalized to $2|\underline{H}_i|$.

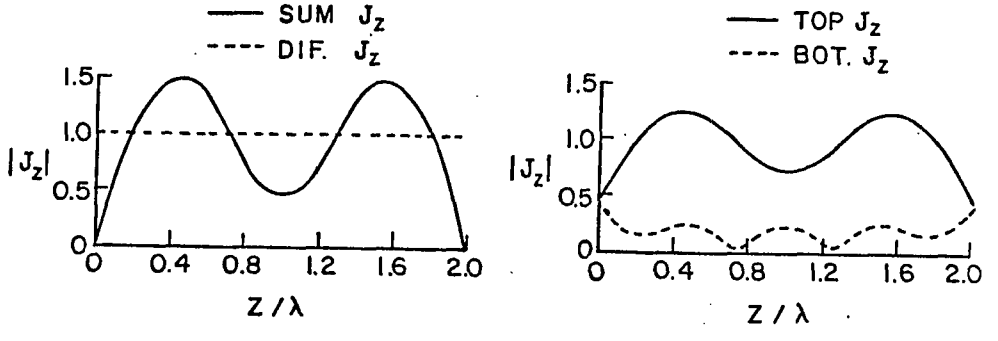

Figure 3.8. Currents on a 2.0λ square plate normalized to $2|\underline{H}_i|$.

1. The magnitude of the difference current is $2|\underline{H}_i|$ for all plate sizes and locations on the plate. This is expected upon examining Equation (2.33b). Writing Equation (2.33b) in its integral form,

$$- \iint_{S_T} \underline{E}_t^M \cdot \underline{J}_D \, ds = - \iint_{S_T} \underline{H}_i \cdot \underline{M}_t \, ds \quad . \tag{3.7}$$

From Equation (2.16), on the surface S_T, the tangential component of $\underline{E}_t^M$ is given by

$$\lim_{\gamma_t \to 0} \underline{E}_t^M(S_T) = \hat{n}_T \times \underline{M}_t/2 \quad . \tag{3.8}$$

Combining Equations (3.7) and (3.8) gives

$$- \iint_{S_T} (\hat{n}_T \times \underline{M}_t) \cdot \underline{J}_D \, ds = - 2 \iint_{S_T} (\underline{H}_i \cdot \underline{M}_t) \, ds \tag{3.9}$$

or

$$\underline{J}_D = 2\hat{n}_T \times \underline{H}_i \quad . \tag{3.10}$$

2. As the plate size, L, increases, the top current generally increases and the bottom current generally decreases. For large plates, the sum and top currents oscillate about the physical optics current. At the plate edges, the magnitude of the normal component of the top and bottom currents are identically $|\underline{H}_i|$. However,

as required by continuity of current, they are 180° out of phase, and thus the normal component of the sum current is zero at the edge.

3. The current on electrically small plates does not go to zero. Rather, the top and bottom currents are nearly equal in magnitude but 180° out of phase. Their magnitude approaches $|\underline{H}_i|$ as L goes to zero. The sum current does go to zero as L goes to zero, however. This behavior is illustrated in Figure 3.4 where $L = 0.125\lambda$.

Next, numerical results for electromagnetic scattering by material plates will be presented. The results, computed using Equations (3.3), (3.4) and (3.5) will be compared with measurements or other computations.

Figure 3.9 shows the radar cross section (RCS) versus angle of incidence for a 0.813λ square by 0.051λ thick penetrable dielectric plate with relative dielectric constant, $\varepsilon_r = \varepsilon/\varepsilon_0 = 4$. Both TE and TM polarizations are shown and compared with measurements by Thal and Finger [34]. The agreement is seen to be good, especially near broadside. This is to be expected, since the surface impedance relationships were evaluated for a normally incident wave. Also shown in Figure 3.9 is the RCS computed by the impedance sheet approximation of Equation (2.41). The sheet impedance approximation produces a less accurate result since it requires $|\gamma t| \ll 1$, while in this case $|\gamma t| = 0.64$.

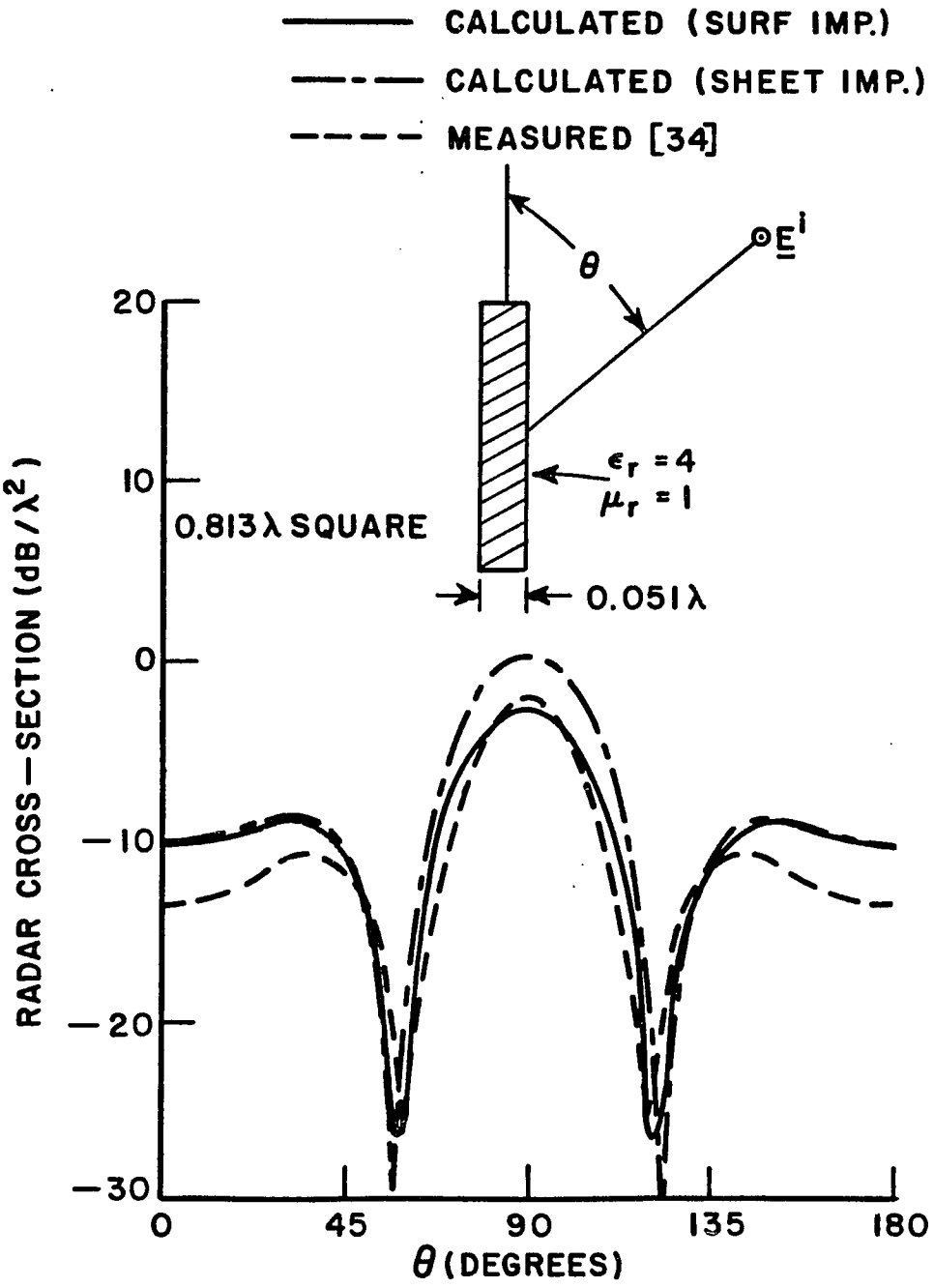

(a) TE scattering.

Figure 3.9. Radar cross section of a 0.813λ square dielectric plate.

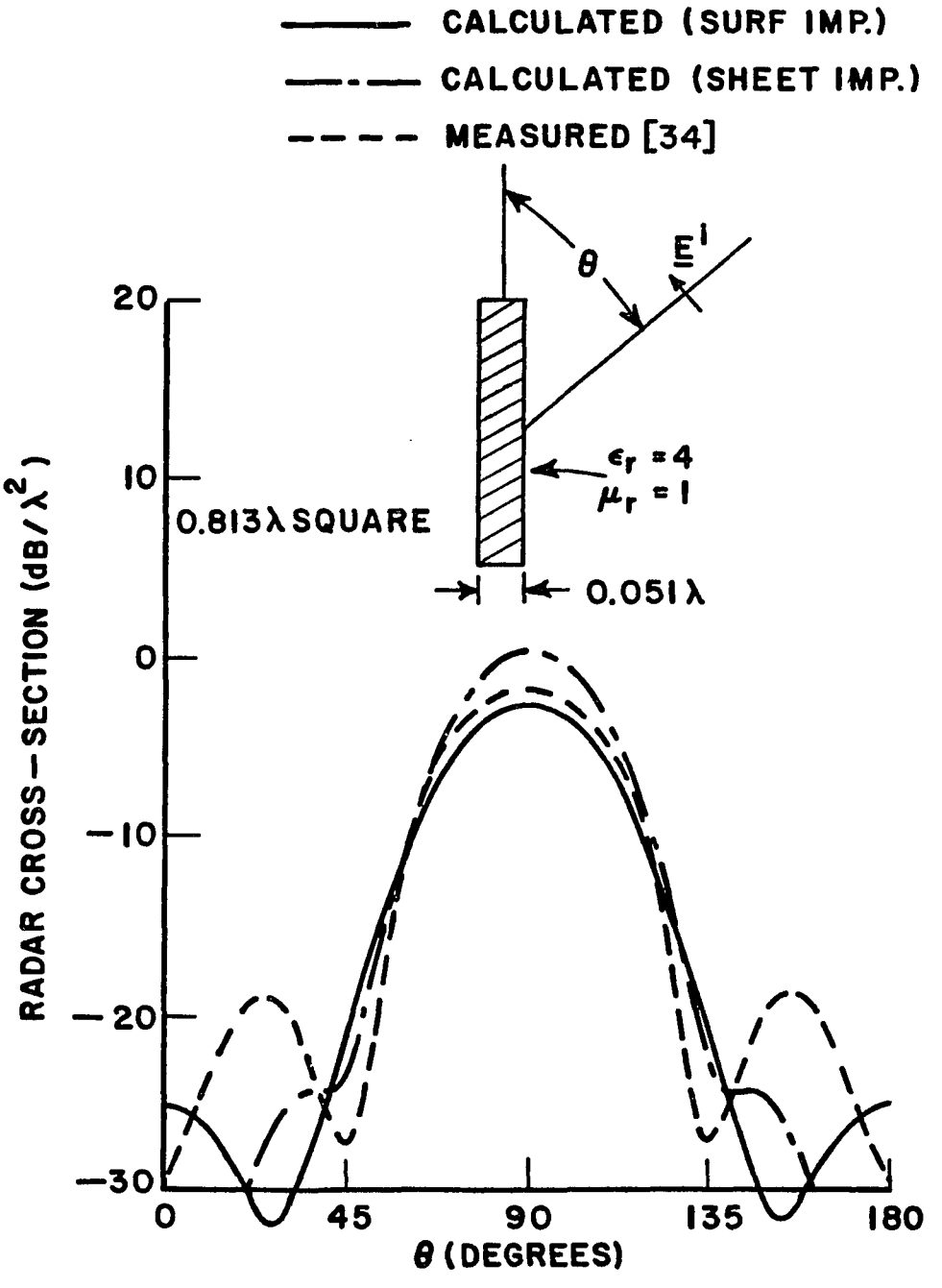

(b) TM scattering.

Figure 3.9. (Continued).

Experience indicates that $|\gamma t|$ should be less than about 0.2 to use the impedance sheet approximation.

Figure 3.10 shows bistatic scattering versus observation angle for the same dielectric plate in Figure 3.9. Both TE and TM polarizations are shown for three different incident angles, θ = 90° (broadside), 45°, and 0° (edge on). The accuracy of Figure 3.10 is unknown, since no other data to compare against could be found. The θ = 0° curves are particularly suspect, since θ = 0° is where the RCS is at its worse.

The insert in Figure 3.11 shows a 1.5λ square perfectly conducting plate coated on one side by a narrow band dielectric/ferrite absorber with ε_r=7.8-j1.6, μ_r=1.5-j0.7, and thickness 0.065λ. This is an example of an impenetrable plate with asymmetric surface impedance relationships. Figure 3.11 shows the RCS of this plate evaluated with the surface impedance relationships of Equation (2.43), and compared with measurements. Note that the theory correctly predicts about a 20 dB drop in RCS when the incident field is broadside to the absorber, rather than the perfect conductor.

Figure 3.12 shows the RCS at broadside for a fiberglass strip dipole of width 0.1λ, thickness 0.032λ, and ε_r = 4.8 versus the dipole length L. Our computation is slightly below the previous computations (based upon the more exact equivalent volume current representation) and measurements of Richmond [35]. Since the surface impedance

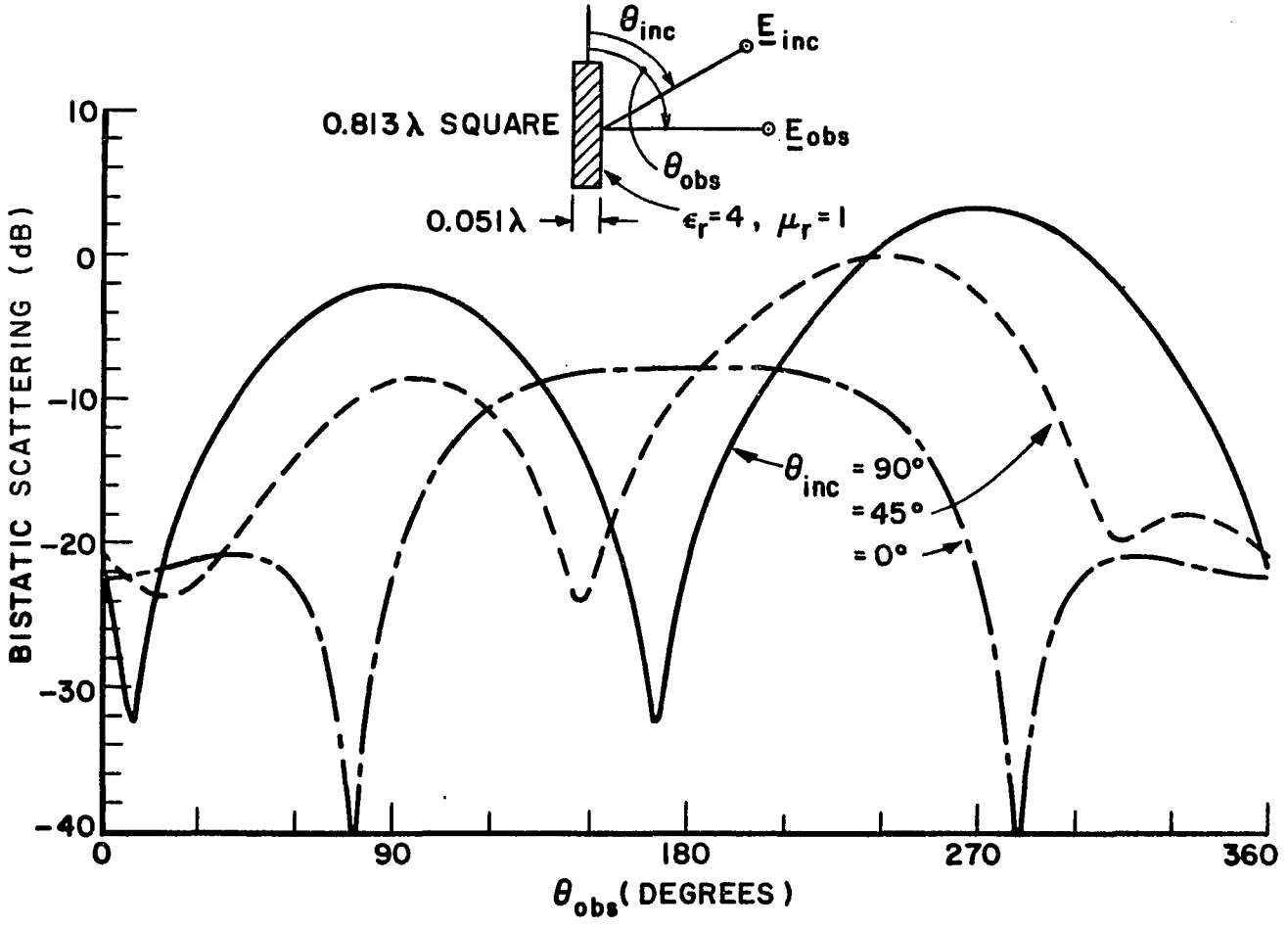

(a) TE scattering.

Figure 3.10. Bistatic scattering from a 0.813λ square dielectric plate.

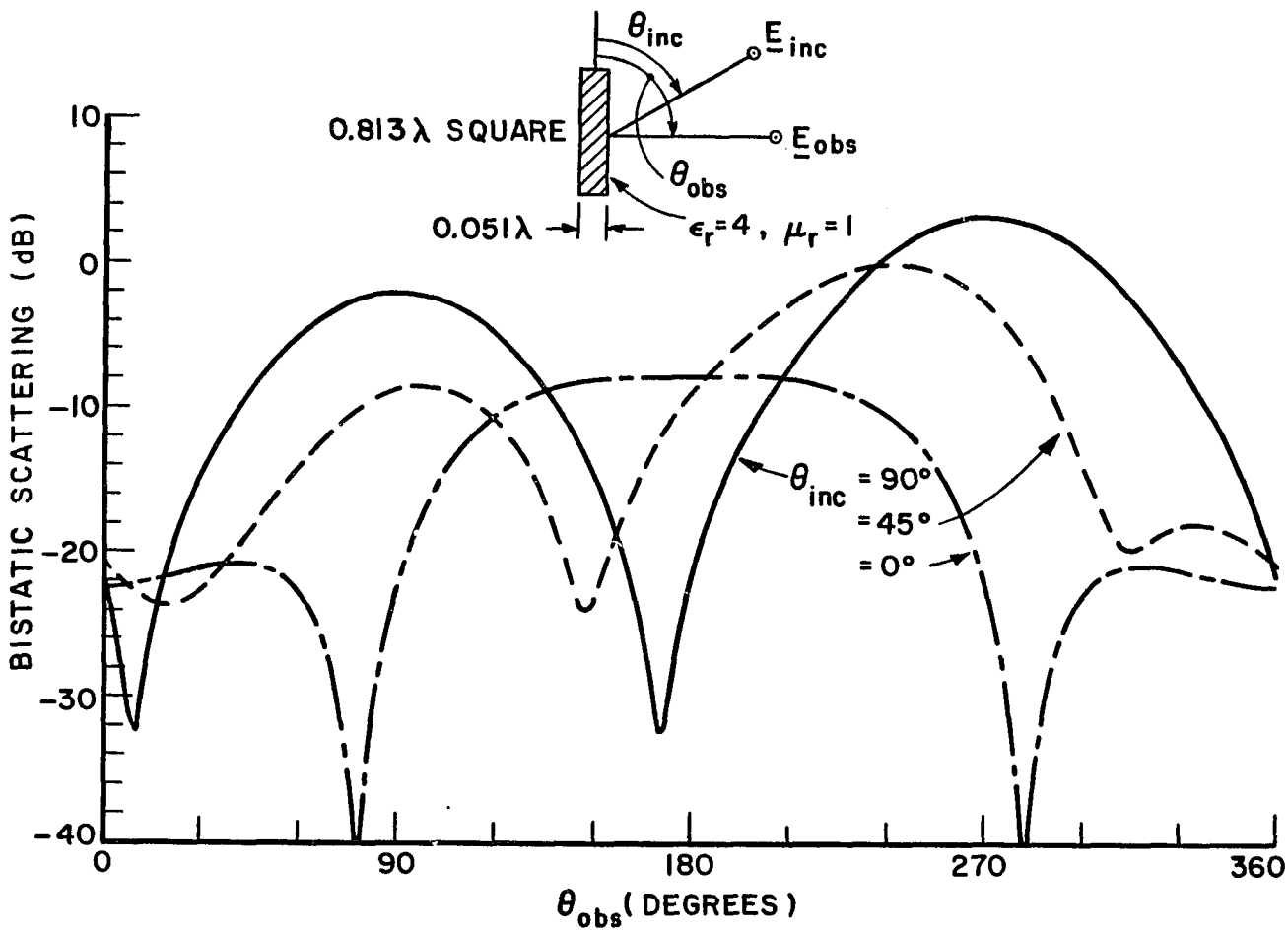

(b) TM scattering.

Figure 3.10. (Continued).

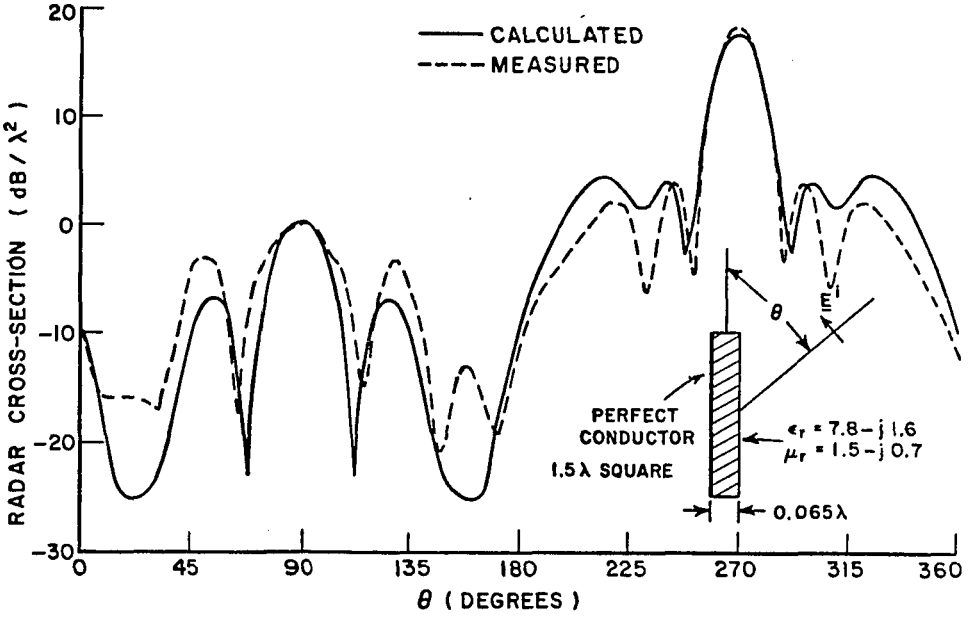

Figure 3.11. TM radar cross section of a 1.5λ square coated, perfectly conducting plate.

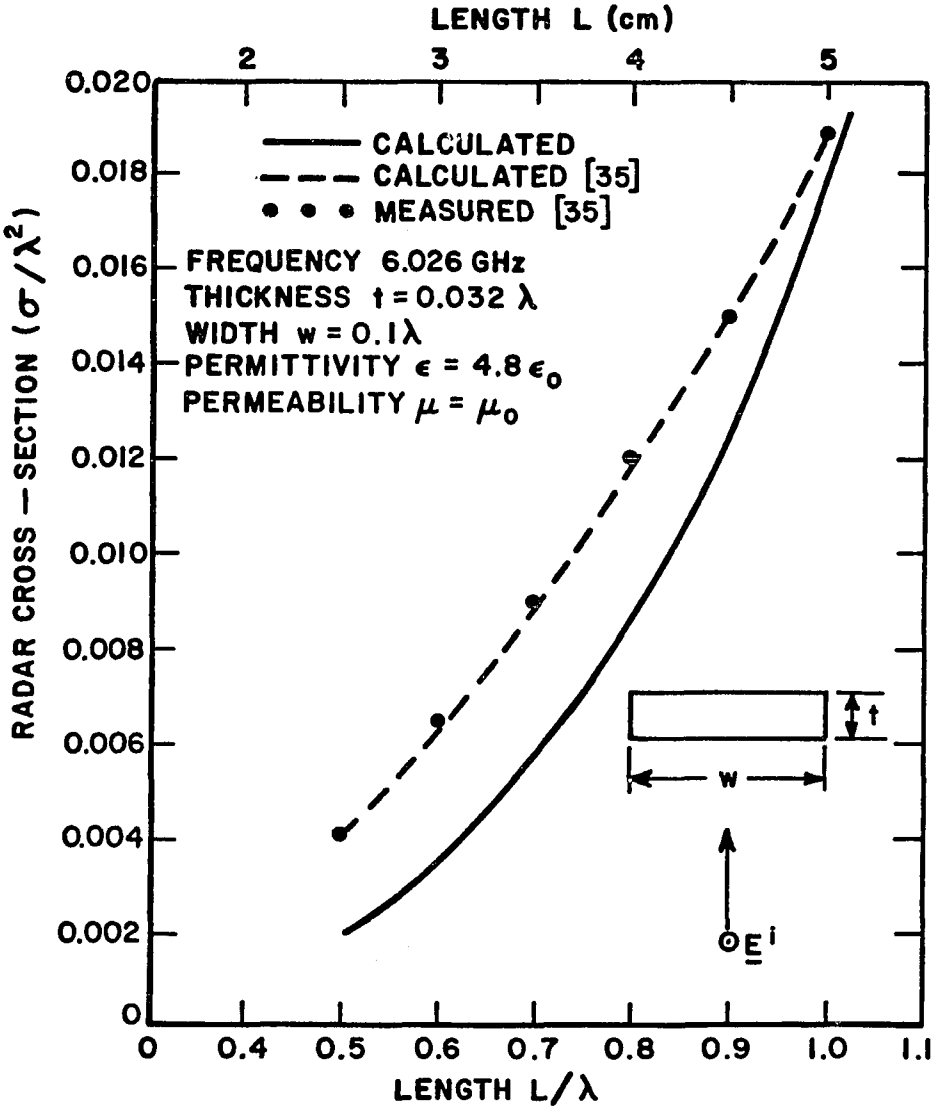

Figure 3.12. Broadside radar cross section of a rectangular fiberglass strip.

approximation is felt to be most accurate away from corners and edges, the degree of error in Figure 3.12 is probably less than one would expect, considering that it is being applied to an extremely narrow plate.

Figure 3.13 shows the RCS at broadside for an aluminum strip dipole of width 0.0056λ, conductivity 35 megamho/meter (i.e., skin depth $\delta = 1.03 \times 10^{-5}\lambda$) versus the dipole length L. Curves are shown for thicknesses of $t = \delta/1000$, $\delta/100$, $\delta/10$, and δ. The agreement between our results and the more exact results of Richmond [35] is seen to be good considering the narrowness of the plate, especially for the larger t values.

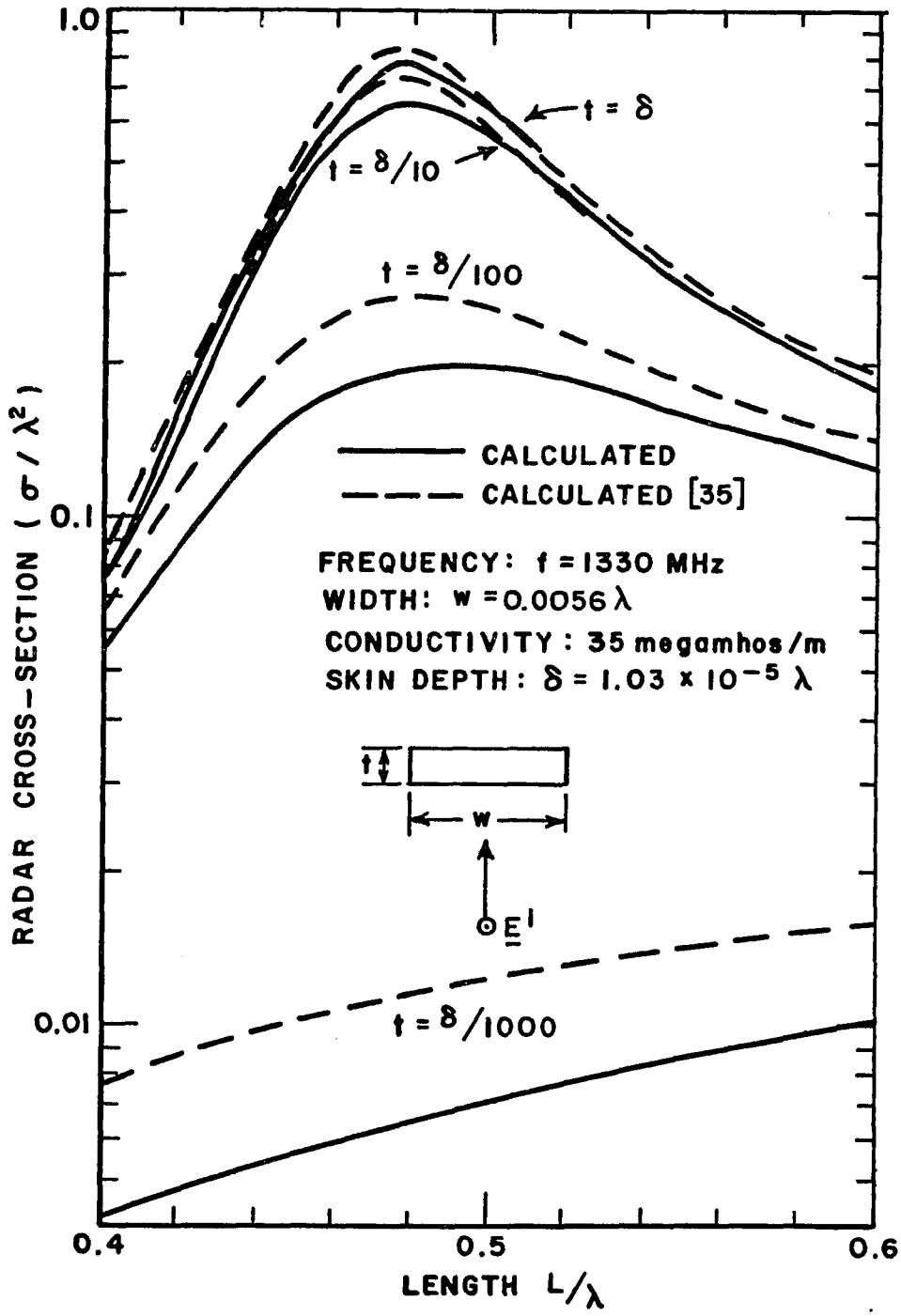

Figure 3.13. Broadside radar cross section of rectangular aluminum strips.

CHAPTER IV

CONCLUSIONS

A solution of electromagnetic scattering by a thin material plate has been presented. The solution has been formulated in such a way so that the integral equation solutions can be most easily integrated into existing computer codes for electromagnetic scattering by perfectly conducting structures. Solutions for the sum and difference electric and magnetic equivalent surface currents are obtained in the form of four coupled integral equations. Two of the four integral equations are approximated by two surface impedance relationships. The surface impedance relationships are shown to be the two-port impedance parameters of simple transmission line models. By allowing for coupling between currents on either side of the plate (i.e., by including the off-diagonal terms in the two port impedance matrix), penetrable as well as impenetrable plates can be treated. The two remaining coupled integral equations were investigated for several special cases, and it was shown that for electrically very thin plates, the results simplify to a single equation equivalent to the impedance sheet approximations used by Harrington and Mautz [19] and Senior [27]. The integral equations were solved by the method of moments and accurate results were

obtained. From the numerical results given in Figure 3.9, it is apparent that accurate results for plate thickness of up to $\lambda/20$ can be obtained. Plate thickness of about $\lambda/10$ should be considered the upper limit, but at that thickness, one could not expect accurate results for incident angles of less than 40 degrees from edge-on. As the plate becomes thinner, the results become more accurate for a wider range of angles. This is evident by the fact that for an electrically very thin plate, the solution reduces to an expression that is equivalent to the impedance sheet approximation, whose accuracy is well established, even for edge-on incidence [27].

There are many topics of further research in this area. All numerical results in this dissertation were based on plane wave incidence. The solution is equally valid for the solution of antenna problems. To solve an antenna problem, one would simply remove the incident field and add a wire and voltage source [13]. The solution would be more useful if it could treat the joining of plates of dissimilar media, particularly the joining of material and perfectly conducting plates. The solution would then be able to treat a wide variety of problems, such as scattering from a terminated absorber over a ground plane or radiation from a microstrip patch antenna. Before the solution can be integrated into a general purpose computer code such as [13], the solution must be extended to include non-planar surfaces. Once the non-planar solution is obtained, one will be able to model general, complex structures (such as that of Figure 1.1) with plates made of any material.

APPENDIX A

NEAR-ZONE FIELDS OF SINUSOIDAL LINE SOURCES

In this Appendix, expressions are given for the near-zone fields of electric and magnetic sinusoidal line sources. While the near-zone fields of an electric sinusoidal line source have been previously published [36], they are included here for completeness.

Consider a line source located on the z axis with endpoints at z_1 and z_2 as shown in Figure A.1. The source has a current distribution given by $\underline{F}(z)$, and the medium is homogeneous with constitutive parameters (μ,ε). Define $\gamma = j\omega\sqrt{\mu\varepsilon}$ as the propagation constant of the medium and $\eta = \sqrt{\mu/\varepsilon}$ as the intrinsic impedance of the medium. Also define $R_i = \sqrt{\rho^2 + (z-z_i)^2}$, $\cos\theta_i = (z-z_i)/R_i$ and $\sin\theta_i = \rho/R_i$ with $i = 1,2$.

A. ELECTRIC LINE SOURCE [36]

Let the line source in Figure A.1 be electric with an electric current distribution given by

$$\underline{F}(z) = \underline{J}(z) = \hat{z}\,\frac{\sinh\gamma(z_2-z)}{\sinh\gamma h} \qquad (A.1)$$

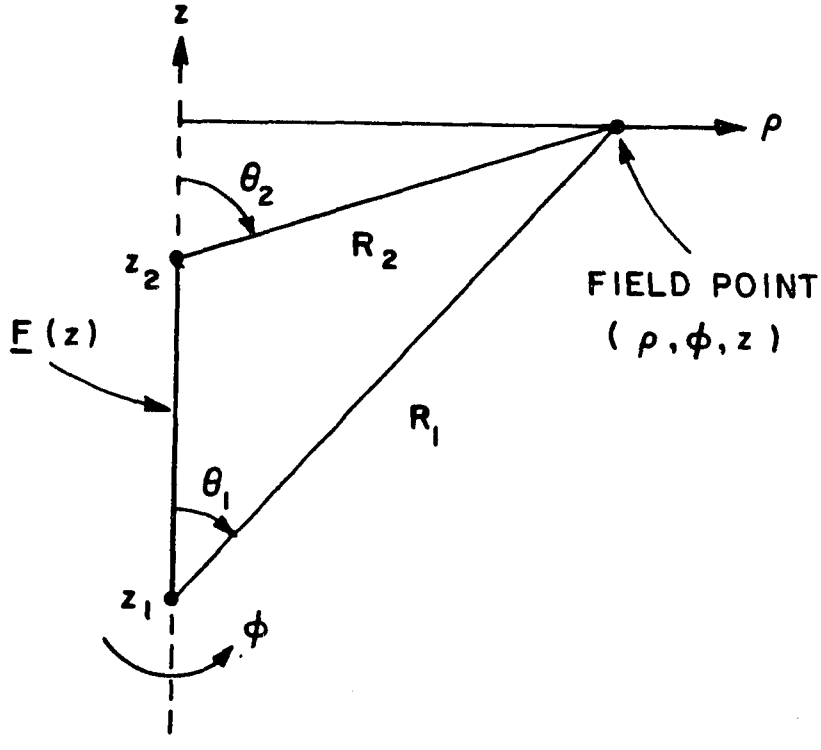

Figure A.1. A line source on the z axis with the observation point (ρ,z).

where $h = z_2 - z_1$, the length of the line source. The cylindrical fields are given by $E_\phi = 0$, $H_\rho = 0$, $H_z = 0$

$$E_\rho = \frac{\eta}{4\pi\rho \sinh\gamma h}\left[(\sinh\gamma h + \cos\theta_1 \cosh\gamma h)e^{-\gamma R1} - \cos\theta_2\, e^{-\gamma R2}\right]$$

$$- \frac{\eta}{4\pi\gamma} \sin\theta_1\, (1 + \gamma R_1)\, e^{-\gamma R1}/R_1^2 \qquad (A.2)$$

$$E_z = \frac{-\eta}{4\pi \sinh\gamma h}\,(\cosh\gamma h\, e^{-\gamma R1}/R_1 - e^{-\gamma R2}/R_2)$$

$$- \frac{\eta}{4\pi\gamma} \cos\theta_1\, (1 + \gamma R_1)\, e^{-\gamma R1}/R_1^2 \qquad (A.3)$$

$$H_\phi = \frac{-1}{4\pi\rho \sinh\gamma h}\left[(\cosh\gamma h + \cos\theta_1\, \sinh\gamma h)\, e^{-\gamma R1} - e^{-\gamma R2}\right]. \qquad (A.4)$$

The last terms in the E_ρ and E_z expressions are the field contributions due to the electric point charges at the endpoints of the line source.

B. MAGNETIC LINE SOURCE

Let the line source in Figure A.1 be magnetic with a magnetic current distribution given by

$$\underline{F}(z) = \underline{M}(z) = \hat{z}\,\frac{\gamma \cosh\gamma(z-z_m)}{2\sinh\gamma w} \tag{A.5}$$

where $z_m = (z_2 + z_1)/2$ is the midpoint of the line source and $w = (z_2 - z_1)/2$ is the half length of the line source. The cylindrical fields are given by $H_\phi = 0$, $E_\rho = 0$, $E_z = 0$

$$H_\rho = \frac{\gamma}{8\pi\eta\rho\sinh\gamma w}\left[(\cosh\gamma w + \cos\theta_1\sinh\gamma w)e^{-\gamma R_1} - (\cosh\gamma w - \cos\theta_2\sinh\gamma w)e^{-\gamma R_2}\right]$$

$$- \frac{\cosh\gamma w}{8\pi\eta\sinh\gamma w}\left[\sin\theta_1(1+\gamma R_1)e^{-\gamma R_1}/R_1^2 - \sin\theta_2(1+\gamma R_2)e^{-\gamma R_2}/R_2^2\right] \tag{A.6}$$

$$H_z = \frac{-\gamma}{8\pi\eta}\left[e^{-\gamma R_1}/R_1 + e^{-\gamma R_2}/R_2\right]$$

$$- \frac{\cosh\gamma w}{8\pi\eta\sinh\gamma w}\left[\cos\theta_1(1+\gamma R_1)e^{-\gamma R_1}/R_1^2 - \cos\theta_2(1+\gamma R_2)e^{-\gamma R_2}/R_2^2\right] \tag{A.7}$$

$$E_{\phi} = \frac{-\gamma}{8\pi\rho \sinh\gamma w} \left[(\sinh\gamma w + \cos\theta_1 \cosh\gamma w)\, e^{-\gamma R1} + (\sinh\gamma w - \cos\theta_2 \cosh\gamma w)\, e^{-\gamma R2} \right] . \qquad (A.8)$$

The last terms in the H_ρ and H_z expressions are the field contributions due to the magnetic point charges at the endpoints of the line source.

APPENDIX B

FAR-FIELD OF SINUSOIDAL SURFACE MONOPOLES

In this appendix, expressions are given for the far-fields of electric and magnetic sinusoidal surface monopoles. The far-field of an electric surface monopole has been previously published [37], however, it is included here for completeness.

From Equations (2.30) and (3.6), the electric and magnetic current densities for monopole 1 in Figure 3.1 are given by

$$\underline{J} = \hat{z}\, F(x,z), \text{ and} \tag{B.1a}$$

$$\underline{M} = \hat{x}\, F(x,z), \text{ respectively,} \tag{B.1b}$$

where

$$F(x,z) = \frac{\gamma \sinh\gamma(z_2-z)\cosh\gamma x}{2\sinh\gamma h\, \sinh\gamma w} \quad , \quad \begin{matrix} -w<x<w \\ z_2<z<z_2 \end{matrix} \tag{B.2}$$

and $h = z_2 - z_1$. The far-fields of Equations (B.1) are given by

$$\underline{E}^J = - \hat{z}_{trans}\ \gamma\eta\ A \tag{B.3a}$$

$$\underline{H}^M = - \hat{x}_{trans}\ \gamma/\eta\ A \tag{B.3b}$$

respectively, where

$$A = \frac{1}{4\pi} \iint_S F(x',z')\ e^{\gamma g}\ dx'\ dz' \tag{B.4}$$

$$g = x' \cos\phi \sin\theta + z' \cos\theta \tag{B.5}$$

and the transverse components of $\hat{x}$ and $\hat{z}$ are given by

$$\hat{x}_{trans} = \hat{\theta} \cos\theta \sin\phi - \hat{\phi} \sin\phi \tag{B.6a}$$

$$\hat{z}_{trans} = - \hat{\theta}\sin\theta \quad . \tag{B.6b}$$

Equation (B.4) can be integrated and substituted into Equations (B.3) to give

$$\underline{E}^J = \hat{\theta}\ \frac{\gamma\eta}{4\pi}\ \sin\theta\ A_1A_2 \tag{B.7a}$$

$$\underline{H}^M = - \frac{\gamma}{4\pi\eta} (\hat{\theta} \cos\theta \sin\phi - \hat{\phi} \sin\phi)\ A_1A_2 \tag{B.7b}$$

where

$$A_1 = \int_{-w}^{w} \frac{\gamma \cosh \gamma x'}{2 \sinh \gamma w} e^{\gamma x' \cos\phi \sin\theta} \, dx', \tag{B.8}$$

or

$$A_1 = \begin{cases} \dfrac{\gamma w + \sinh \gamma w \cosh \gamma w}{2 \sinh \gamma w}, & |\cos\phi \sin\theta| = 1 \\ \dfrac{\sinh \gamma w \cosh(\gamma w \cos\phi \sin\theta) - \cos\phi \sin\theta \cosh \gamma w \sinh(\gamma w \cos\phi \sin\theta)}{\sinh \gamma w (1 - \cos^2\phi \sin^2\theta)}, & \text{otherwise} \end{cases} \tag{B.9}$$

and

$$A_2 = \int_{z_1}^{z_2} \frac{\sinh \gamma (z_2 - z')}{\sin \gamma h} e^{\gamma z' \cos\theta} \, dz' , \quad \text{or} \tag{B.10}$$

$$A_2 = \begin{cases} -\dfrac{e^{\gamma z_2 \cos\theta}}{4 \gamma \sinh \gamma h} \left[1 - e^{-2\gamma h \cos\theta} - 2\gamma h \cos\theta \right], & |\cos\theta| = 1 \\ -\dfrac{e^{\gamma z_2 \cos\theta}}{\gamma \sinh \gamma h \sin^2\theta} \left[1 - e^{-\gamma h \cos\theta} (\cosh \gamma h + \cos\theta \sinh \gamma h) \right], & \text{otherwise} . \end{cases} \tag{B.11}$$

APPENDIX C

EVALUATION OF IMPEDANCE ELEMENTS

A. INTRODUCTION

This appendix will discuss the evaluation of the impedance elements in Equation (3.4). As shown in Figure 3.1, each surface patch dipole mode consists of two surface patch monopoles. Therefore, each dipole-to-dipole impedance element is the sum of four surface monopole-to-surface monopole impedances. Exceptions occur when either of the surface patch modes is an edge mode, since an edge mode consists of only one surface monopole. However, in any case, all modal impedance elements are evaluated as a sum of monopole-to-monopole impedances. Thus, the expressions for the monopole-to-monopole impedance will be presented here.

Figure C.1 shows two arbitrary surface monopoles. The currents on each monopole can be either electric or magnetic. The vector direction of the current is $\hat{s}_1$ on the test monopole and $\hat{t}_1$ on the expansion monopole. The surface monopole-to-surface monopole impedance, Z_{mn}, of the surface monopoles in Figure C.1 is given by

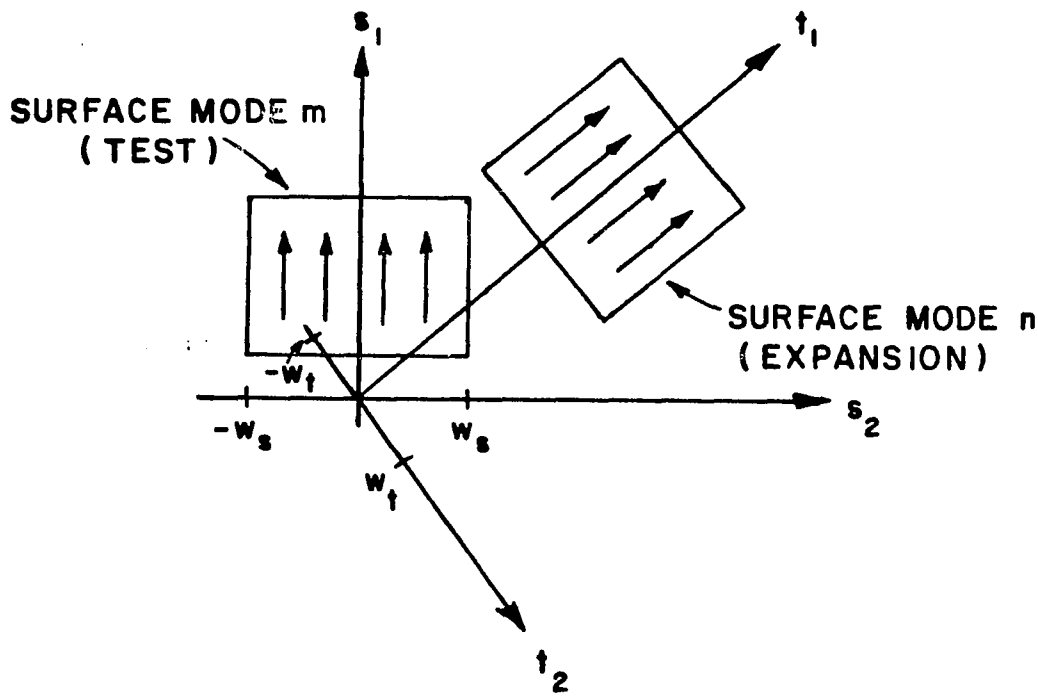

Figure C.1. Geometry of two arbitrary surface monopoles.

$$Z_{mn} = - \int_{t_1} \int_{t_2} [\underline{E}_m(t_1,t_2)\cdot\underline{J}_n(t_1,t_2) - \underline{H}_m(t_1,t_2)\cdot\underline{M}_n(t_1,t_2)]dt_1\ dt_2, \tag{C.1}$$

where $\underline{E}_m$ and $\underline{H}_m$ are the free space electric and magnetic fields of the test surface monopole and $\underline{J}_n$ and $\underline{M}_n$ are the electric and magnetic current densities of the expansion surface monopole. If the expansion surface monopole is electric, then $\underline{M}_n = 0$; if the expansion surface monopole is magnetic, then $\underline{J}_n = 0$. If the test mode is electric, then its free space fields are given by

$$\underline{H}_m(t_1,t_2) = \nabla x \int_{s_1} \int_{s_2} \underline{J}_m(s_1,s_2)\ G_o(t_1,t_2;s_1,s_2)\ ds_1\ ds_2 \tag{C.2a}$$

$$E_m(t_1,t_2) = \frac{\eta_o}{\gamma_o} \nabla x\ \underline{H}_m(t_1,t_2) \tag{C.2b}$$

where $G_o = \frac{e^{-\gamma_o R}}{4\pi R}$ is the free space Green's function, γ_o is the propagation constant of free space, and η_o is the intrinsic impedance of free space. If the test mode is magnetic, then its free space fields are given by

$$\underline{E}_m(t_1,t_2) = - \nabla x \int_{s_1} \int_{s_2} \underline{M}_m(s_1,s_2)\ G_o(t_1,t_2;s_1,s_2)\ ds_1\ ds_2 \tag{C.3a}$$

$$\underline{H}_m(t_1,t_2) = - \frac{1}{\gamma_o \eta_o} \nabla x\ \underline{E}_m(t_1,t_2) \quad . \tag{C.3b}$$

From Equations (C.1), (C.2) and (C.3), it is seen that the evaluation of an element requires a four fold integration. The impedance elements could be evaluated by the method outlined above, i.e., computing the fields of the test surface monopole and evaluating the mutual impedance with the expansion surface monopole. However, it has been shown [37] that it is usually more convenient and efficient to rearrange the order of integration to give

$$Z_{mn} = \int_{s_2} F_s(s_2) \int_{t_2} F_t(t_2)\, z_{mn}(s_2,t_2)\, ds_2\, dt_2 \qquad (C.4)$$

where $F_s(s_2)$ and $F_t(t_2)$ represent the weighting functions of the current distributions in the direction orthogonal to the current vector direction on the test and expansion modes, respectively, and $z_{mn}(s_2,t_2)$ is the mutual impedance between two current filaments lying in the s_1 and t_1 directions. For example, if both surface monopoles are electric then

$$F_s(s_2) = \frac{\gamma \cosh\gamma(s_2-w_s)}{2\sinh\gamma w_s} \quad , \qquad (C.5a)$$

$$F_t(t_2) = \frac{\gamma \cosh\gamma(t_2-w_t)}{2\sinh\gamma w_t} \quad , \qquad (C.5b)$$

and the filament-to-filament mutual impedance is given by

$$z_{mn}^{EE}(s_2,t_2) = \int_{t_1} \underline{J}_{t_1}(t_1,t_2) \cdot \underline{E}_{s_1}(s_2,t_1,t_2)\, dt_1 \qquad (C.5c)$$

where $\underline{J}_{t_1}$ is the expansion electric current filament flowing in the $\hat{t}_1$ direction and $\underline{E}_{s_1}$ is the electric field of $\underline{J}_{s_1}$, the test electric current filament flowing in the $\hat{s}_1$ direction with

$$\underline{E}_{s_1}(s_2,t_1,t_2) = \frac{\eta_o}{\gamma_o} \nabla x \nabla x \int_{s_1} \underline{J}_{s_1}(s_1,s_2)\, G_o(t_1,t_2;s_1,s_2)\, ds_1 \,. \tag{C.6}$$

Impedance expressions for electric filament-to-magnetic filament, magnetic filament-to-electric filament, and magnetic filament-to-magnetic filament are derived in the same way. In the remaining sections of this appendix, complete filament-to-filament impedance expressions will be derived. Although electric filament-to-electric filament impedance expressions have been previously published [38,39], they are included here for completeness. In addition, an electric surface monopole-to-magnetic surface monopole impedance expression is derived for a special case.

B. FILAMENT-TO-FILAMENT IMPEDANCE EXPRESSIONS

Consider the two filaments imersed in homogeneous medium as shown in Figure C.2 for non-planar skew filaments and Figure C.3 for parallel filaments. The test filament is located on the z axis with endpoints at z_1 and z_2. Also, let $h_s = z_2-z_1$ be the length, $w_s = (z_2-z_1)/2$ be the half length, and $z_m = (z_2+z_1)/2$ be the midpoint of the test filament. The expansion filament is on the t axis, which lies in the y = d plane, and has endpoint at t_1 and t_2. Also let $h_t = t_2-t_1$ be

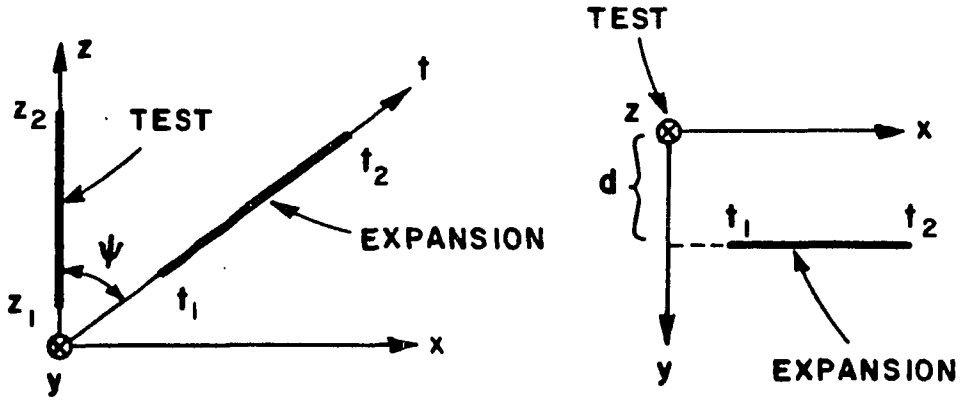

(a) x-z plane view. (b) x-y plane view.

Figure C.2. Coordinate system for two non-planar skew filaments.

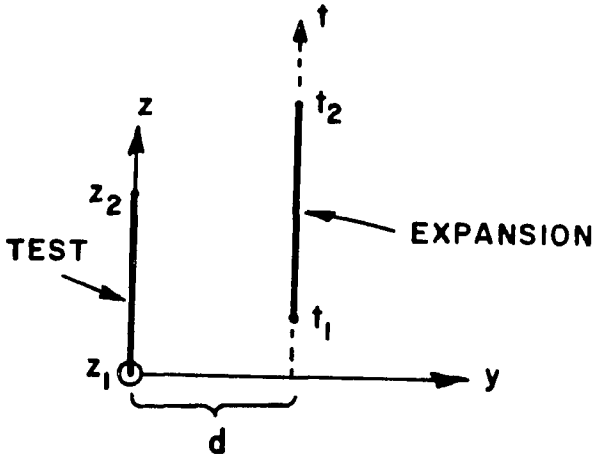

Figure C.3. Coordinate system for two parallel filaments.

the length, $w_t = (t_2-t_1)/2$ be the half length, and $t_m = (t_2+t_1)/2$ be the midpoint of the expansion filament. Lastly, define γ as the propagation constant and η as the intrinsic impedance of the medium.

1. Electric-to-Electric Filaments

If both filaments in Figures C.2 or C.3 are electric, then the electric current density and fields of the test filament are given in Equations (A.1), (A.2) and (A.3) and the electric current density of the expansion filament is given by

$$\underline{J}_t = \hat{t} \frac{\sinh\gamma(t_2-t)}{\sinh\gamma h_t} \quad , \tag{C.7}$$

where $h_t = t_2-t_1$.

Combining Equations (C.5c) and (C.7) yields

$$z_{mn}^{EE} = - \int_{t_1}^{t_2} \frac{\sinh\gamma(t_2-t)}{\sinh\gamma h_t} \left(\frac{x}{\rho} \sin\psi \, E_\rho + \cos\psi \, E_z\right) dt \quad , \tag{C.8}$$

where E_z and E_ρ are given in Equations (A.2) and (A.3), respectively. In order to simplify the algebra, the expressions for the electric fields E_ρ and E_z will have the contribution due to the electric point charges at the endpoints of the test filament removed. The mutual impedance between the expansion current and the test point charges will be computed separately. The total mutual impedance between two electric filaments with end charges included will be the sum of the two impedances.

Non-Planar Skew Filaments [38]: Expanding Equation (C.8) with Equations (A.2) and (A.3) (end charges removed) yields

$$z_{mn}^{EE} = \frac{-\eta}{8\pi \sinh\gamma h_s \sinh\gamma h_t} \int_{t_1}^{t_2} [e^{\gamma(t_2-t)} - e^{-\gamma(t_2-t)}]$$

$$\cdot \left[\frac{x\sin\psi}{\rho^2} \left((\sinh\gamma h_s + \frac{z-z_1}{R_1} \cosh\gamma h_s)\, e^{-\gamma R_1} - \frac{z-z_2}{R_2} e^{-\gamma R_2} \right) \right.$$

$$\left. -\cos\psi (\cosh\gamma h_s\, e^{-\gamma R_1}/R_1 - e^{-\gamma R_2}/R_2) \right] dt \qquad (C.9)$$

where R_i can be written as

$$R_i = \sqrt{z_i^2 + t^2 - 2z_i t \cos\psi + d^2} \quad . \qquad (C.10)$$

Let

$$P_i^s = 2\int_{t_1}^{t_2} \frac{e^{s\gamma t}\, e^{-\gamma R_i}}{R_i} \left[\cos\psi - \frac{x(z-z_i)\sin\psi}{\rho^2} \right] dt \qquad (C.11a)$$

$$Q_i^s = 2 \sin\psi \int_{t_1}^{t_2} \frac{x}{\rho^2} e^{s\gamma t}\, e^{-\gamma R_i}\, dt \qquad (C.11b)$$

with $s = \pm 1$ and $i = 1,2$.

Rewriting Equation (C.9) in terms of P_i^s and Q_i^s yields

$$z_{mn}^{EE} = \frac{-\eta}{16\pi \sinh\gamma h_s \sinh\gamma h_t} \left[e^{\gamma t2} \left(\sinh\gamma h_s Q_1^- - \cosh\gamma h_s P_1^- + P_2^-\right) \right.$$

$$\left. - e^{-\gamma t2} \left(\sinh\gamma h_s Q_1^+ - \cosh\gamma h_s P_1^+ + P_2^+\right) \right] . \qquad (C.12)$$

Define the E function as

$$E(\alpha+j\beta) = e^{j\gamma\beta} \int_{\alpha_1+j\beta}^{\alpha_2+j\beta} \frac{e^{-\gamma w}}{w} \, dw \qquad (C.13)$$

where α and β are real quantities with dimensions of length, and $\alpha_i = \alpha(t_i)$ is a function of t. The integral in Equation (C.13) may be expressed in terms of exponential integrals as

$$S = \int_{v_1}^{v_2} \frac{e^{-v}}{v} \, dv = E_1(v_1) - E_1(v_2) + j2n\pi \quad . \qquad (C.14)$$

The integration path in Equation (C.14) is a straight line from v_1 to v_2 in the v plane. The integer n is zero unless this path intersects the negative real v axis. When there is such an intersection, n=1 if v_1 lies above the real axis and n=-1 if v_1 lies below the real axis. P_i^S and Q_i^S can now be written as

$$P_i^S = e^{-\gamma z_i} E(x_{1i}^S) - e^{\gamma z_i} E(x_{2i}^S) + e^{-\gamma z_i} E(x_{3i}^S) - e^{\gamma z_i} E(x_{4i}^S) \qquad (C.14a)$$

$$Q_i^s = e^{-\gamma z_i} E(x_{1i}^s) + e^{\gamma z_i} E(x_{2i}^s) + e^{-\gamma z_i} E(x_{3i}^s) + e^{\gamma z_i} E(x_{4i}^s)$$
$$- 2e^{s\gamma z_i \cos\psi} E(x_{5i}^s) \qquad \text{(C.15b)}$$

where the integration paths are defined by

$$x_{1i}^s = R_i - st - z_i + j(\cos\psi + s)\, d/\sin\psi \qquad \text{(C.16a)}$$

$$x_{2i}^s = R_i - st + z_i - j(\cos\psi - s)\, d/\sin\psi \qquad \text{(C.16b)}$$

$$x_{3i}^s = R_i - st - z_i - j(\cos\psi + s)\, d/\sin\psi \qquad \text{(C.16c)}$$

$$x_{4i}^s = R_i - st + z_i + j(\cos\psi - s)\, d/\sin\psi \qquad \text{(C.16d)}$$

$$x_{5i}^s = R_i - st + 2z_i \cos\psi \quad . \qquad \text{(C.16e)}$$

Finally, define

$$F_i^s = 2e^{-s\gamma z_i \cos\psi} E(x_{si}^s) \qquad \text{(C.17a)}$$

$$G_1^s = E(x_{12}^s) + E(x_{32}^s) - E(x_{11}^s) - E(x_{31}^s) \qquad \text{(C.17b)}$$

$$G_2^s = E(x_{22}^s) + E(x_{42}^s) - E(x_{21}^s) - E(x_{41}^s) \; . \qquad \text{(C.17c)}$$

Combining Equations (C.12), (C.15) and (C.17) yields

$$z_{mn}^{EE} = \frac{\eta}{16\pi \sinh\gamma h_s \sinh\gamma h_t} \left[e^{\gamma t_2} \left(\sinh\gamma h_s \, F_1^- - e^{-\gamma z_2} \, G_1^- + e^{\gamma z_2} \, G_2^-\right) \right.$$

$$\left. - e^{-\gamma t_2} \left(\sinh\gamma h_2 \, F_1^+ - e^{-\gamma z_1} \, G_1^+ + e^{\gamma z_2} \, G_2^+\right) \right] \quad . \tag{C.18}$$

Parallel Filaments [39]: If the filaments are parallel ($\sin\psi=0$), then Equation (C.8) can be expanded with Equation (A.3) (end charges removed) to give

$$z_{mn}^{EE} = \frac{\eta\cos\psi}{8\pi\sinh\gamma h_s \sinh\gamma h_t} \int_{t_1}^{t_2} \left(e^{\gamma(t_2-t)} - e^{-\gamma(t_2-t)}\right)$$

$$\cdot \left(\cosh\gamma h_s \, e^{-\gamma R_1}/R_1 - e^{-\gamma R_2}/R_2\right) dt \ , \tag{C.19}$$

where

$$R_i = \sqrt{(t-z_i\cos\psi) + d^2} \quad , \quad i = 1,2 \ ; \ \cos\psi = \pm 1 \quad . \tag{C.20}$$

Just as in Equation (C.11a), let

$$P_i^s = 2 \int_{t_1}^{t_2} e^{s\gamma t} \, e^{-\gamma R_i}/R_i \, dt \tag{C.21}$$

with $s = \pm 1$, $i = 1,2$.

Rewriting Equation (C.19) in terms of P_i^s gives

$$z_{mn}^{EE} = \frac{\eta \cos\psi}{16\pi \sinh\gamma h_s \sinh\gamma h_t} \left[e^{\gamma t 2} \left(\cosh\gamma h_s \; P_1^- - P_2^-\right) \right.$$

$$\left. -e^{-\gamma t 2} \left(\cosh\gamma h \;\; P_1^+ - P_2^+\right) \right] \quad . \tag{C.22}$$

In Equation (C.21), let

$$u = R_i - s(t - z_i \cos\psi) \text{ , and} \tag{C.23a}$$

$$du = -s \; u/R_i \; du \quad . \tag{C.23b}$$

Then Equation (C.21) can be integrated to give

$$P_i^s = - 2s \; e^{s\gamma z_i \cos\psi} \; E(x_i^s) \tag{C.24}$$

where the E function is defined in Equations (C.13) and (C.14) and the integration interval is

$$x_i^s = R_i - s(t - z \cos\psi) \tag{C.25}$$

with R_i as defined in Equation (C.20), i = 1,2 and s = ±1.
Substituting Equation (C.24) into Equation (C.22) gives

$$Z_{mn}^{EE} = \frac{-\eta\cos\psi}{8\pi\sinh\gamma h_s \sinh\gamma h_t}\left[e^{\gamma(t_2-z_2\cos\psi)}E(x_2^-) + e^{-\gamma(t_2-z_2\cos\psi)}E(x_2^+) \right.$$

$$\left. -\cosh\gamma h_s\left(e^{\gamma(t_2-z_1\cos\psi)}E(x_1^-) + e^{-\gamma(t_2-z_1\cos\psi)}E(x_1^+)\right)\right] . \quad (C.26)$$

Point Charge Contribution [40]: From Equations (A.2) and (A.3), the electric field due to the point charges at the endpoints of the test electric filament are

$$\underline{E}_s = -\frac{\eta}{4\pi\gamma}\hat{R}_1\,(1+\gamma R_1)\,e^{-\gamma R_1}/R_1 \quad (C.27)$$

where $\hat{R}_1 = \hat{\rho}\sin\theta_1 + \hat{z}\cos\theta_1$ is a unit vector pointing from the point charge at z_1 to the field point. Combining Equations (C.5c) and (C.27), the point charge contribution of the mutual impedance of two electric filaments is

$$Z_{mn}^{EE} = \frac{\eta}{4\pi\gamma\sinh\gamma h_t}\int_{t_1}^{t_2}(\hat{t}\cdot\hat{R}_1)\sinh\gamma(t_2-t)(1+\gamma R_1)e^{-\gamma R_1}/R_1^2\,dt \quad (C.28)$$

with

$$R_1 = \sqrt{z_1^2+t^2-2z_1t\cos\psi+d^2} = \sqrt{(t-z_1\cos\psi)^2+(z_1\sin\psi)^2+d^2} . \quad (C.29)$$

Integrating Equation (C.28) by parts, let

$$dv = (\hat{t}\cdot\hat{R}_1)(1+\gamma R_1)e^{-\gamma R_1}/R_1^2\,dt \quad (C.30a)$$

$$u = \sinh\gamma(t_2-t) \quad . \tag{C.30b}$$

Since $\hat{t}\cdot\hat{R}_1 = (t-z_i\cos\psi)/R_i = \frac{\partial}{\partial t} R_i$, Equation (C.30a) can be written as

$$dv = \frac{\partial}{\partial t} \left(-e^{-\gamma R_1}/R_1\right) dt \quad . \tag{C.31}$$

In addition

$$v = -e^{-\gamma R_1}/R_1 \tag{C.32a}$$

$$du = -\gamma\cosh\gamma(t_2-t)\, dt. \tag{C.32b}$$

Carrying out the integration in Equation (C.28),

$$z_{mn}^{EE} = \frac{\eta}{4\pi\gamma\sinh\gamma h_t} \left[-\sinh\gamma(t_2-t)\, e^{-\gamma R_1}/R_1 \Big|_{t_1}^{t_2} - \gamma \int_{t_1}^{t_2} \cosh\gamma(t_2-t)\, e^{-\gamma R_1}/R_1\, dt \right] , \tag{C.33}$$

or

$$z_{mn}^{EE} = \frac{\eta}{4\pi\gamma} e^{-\gamma R_1(t_1)}/R_1(t_1) - \frac{\eta}{16\pi\sinh\gamma h_t} \left[e^{\gamma t_2}\, p_1^- + e^{-\gamma t_2}\, p_1^+ \right] \tag{C.34}$$

where P_i^s is defined in Equation (C.21) with R_i as defined in Equation (C.29). Following a procedure similar to Equations (C.21) - (C.24), P_i^s is given as

$$P_i^s = - 2s\, e^{s\gamma z_i \cos\psi}\, E(x_i^s) \tag{C.35}$$

where the E function is defined in Equations (C.13) and (C.14) and the integration interval is

$$x_i^s = R_i - s(t - z_i \cos\psi) \ , \tag{C.36}$$

with R_i as defined in Equation (C.29). Combining Equations (C.34) and (C.35) yields

$$z_{mn}^{EE} = \frac{\eta}{4\pi\gamma}\, e^{-\gamma R_1(t_1)}/R_1(t_1) + \frac{\eta}{8\pi \sinh\gamma h_t} \left[\int_-^- e^{-\gamma(t_2 - z_1\cos\psi)}\, E(x_1^+) - e^{\gamma(t_2 - z_1\cos\psi)}\, E(x_1^-) \right]_-^- \ . \tag{C.37}$$

2. Electric-to-Magnetic, Magnetic-to-Electric Filaments

If the test filament in Figure C.2 or C.3 is electric and the expansion filament is magnetic, then the electric current density and

fields of the test filament are given in Equations (A.1) -(A.4) and the magnetic current density of the expansion filament is given by

$$\underline{M}_t = \hat{t}\,\frac{\gamma\cosh\gamma(t-t_m)}{2\sinh\gamma w_t} \quad , \tag{C.38}$$

where $t_m=(t_2+t_1)/2$ and $w_t=(t_2-t_1)/2$. If, on the other hand, the test filament in Figure C.2 or C.3 is magnetic and the expansion filament is electric, then the magnetic current density and fields of the test filament are given in Equations (A.5) - (A.8) and the electric current density of the expansion filament is given by

$$\underline{J}_t = \hat{t}\,\frac{\sinh\gamma(t_2-t)}{\sinh\gamma h_t} \quad , \tag{C.39}$$

where $h_t=t_2-t_1$. However, by reciprocity [29], which filament is called the test filament and which filament is called the expansion filament are interchangeable. In other words, if say, test filament m is electric and expansion filament n is mangetic, then the mutual impedance will be the same as if expansion filament m is electric and test filament n is magnetic, i.e.,

$$z_{mn}^{EM} = z_{nm}^{ME} \quad . \tag{C.40}$$

Therefore, it is necessary to derive expressions for either z^{EM} or z^{ME}, not both. In this Appendix, z^{EM} is arbitrarily chosen. Combining Equations (A.4) and (C.38) and observing from Figure C.2 that $\hat{t}\cdot\hat{\phi} = -d\sin\psi/\rho$

$$z_{mn}^{EM} = z_{nm}^{ME} = \int_{t_1}^{t_2} \frac{d\sin\psi}{\pi\rho^2} \frac{\gamma\cosh\gamma(t-t_m)}{2\sinh\gamma w_t} \frac{1}{4\sinh\gamma h_s}$$

$$\left[(\cosh\gamma h_s + \frac{z-z_1}{R_1} \sinh\gamma h_s)\, e^{-\gamma R_1} - e^{-\gamma R_2} \right] dt \ . \qquad (C.41)$$

As of yet, no method of evaluating the integral in Equation (C.41), other than numerical integration, has been found. However, two special cases can be evaluated:

$$z_{mn}^{EM} = z_{nm}^{ME} = 0 \ , \ \sin\psi = 0 \text{ (parallel filaments)} \qquad (C.42)$$

and

$$\lim_{d\to 0} z_{mn}^{EM} = \lim_{d\to 0} z_{nm}^{ME} = \begin{cases} \text{sgn}(d)\, \dfrac{\gamma\cosh\gamma t_m \sinh\gamma z_2}{4\sinh\gamma w_t \sinh\gamma h_s} & z_1, t_1 < 0 < z_2, t_2 \\ 0 & \text{otherwise} \end{cases} \qquad (C.43)$$

where sgn(x) = 1 if x>0 and -1 if x<0 .

3. Electric-to-Magnetic, Magnetic-to-Electric Surface Monopoles

In general, the mutual impedance of a magnetic surface monopole and an electric surface monopole must be calculated via Equations (C.4) and (C.41). However, if the two surface monopoles are planar (i.e., the surface monopoles are parallel and their separation, d, approaches zero), a closed form expression can be obtained. For planar surface

monopoles, the filament-to-filament mutual impedance in Equation (C.43) applies. It can be seen from examining Equations (C.42) and (C.43) that the mutual impedance between two surface monopoles is zero if the two surface monopoles do not overlap and if the current vectors are parallel. Planar patches overlap with non-parallel current vectors only in two cases: when calculating the self impedance of a surface monopole (for example, the self impedance of surface monopole 1 in Figure 3.1), and when calculating the mutual impedance between two adjacent surface dipole modes that share one monopole (for example, the mutual impedance between surface dipole modes 11 and 12 in Figure 3.2). For the self impedance of a surface monopole, from Equations (C.4) and (C.43),

$$Z_{mm}^{EM} = Z_{mm}^{ME} = \frac{sgn(d)}{4} \int_{z_1}^{z_2} \left(\frac{\sinh\gamma(z_2-z)}{\sinh\gamma h}\right)^2 dz \int_{-w}^{w} \left(\frac{\gamma\cosh\gamma x}{2\sinh\gamma w}\right)^2 dx \ , \qquad (C.44)$$

or

$$Z_{mm}^{EM} = Z_{mm}^{ME} = sgn(d)\ \frac{(-\gamma h+\cosh\gamma h\ \sinh\gamma h)(\gamma w+\cosh\gamma w\ \sinh\gamma w)}{(4\sinh\gamma h\ \sinh\gamma w)^2} \qquad (C.45)$$

where sgn(x) = 1 if x>0 and -1 if x<0 .

The mutual impedance of overlapping adjacent surface dipole modes is obtained from Equations (C.4) and (C.43) and yields

$$Z_{mn}^{EM} = Z_{nm}^{ME} = \frac{sgn(d)}{4} \int_{z_1}^{z_2} \left(\frac{\sinh\gamma(z_2-z)\sinh\gamma z}{\sinh\gamma h}\right) dz \int_{-w}^{w} \left(\frac{\gamma\cosh\gamma x}{2\sinh\gamma w}\right)^2 dx \ , \qquad (C.46)$$

or

$$z_{mn}^{EM} = z_{nm}^{ME} = \text{sgn}(d)\ \frac{(\sinh^3\gamma h+\gamma h\cosh\gamma h-\cosh^2\gamma h\sinh\gamma h)(\gamma w+\cosh\gamma w\sinh\gamma w)}{(4\sinh\gamma h\ \sinh\gamma w)^2}$$

4. Magnetic-to-Magnetic Filaments

If both filaments in Figure C.2 or C.3 are magnetic, then the magnetic current density and fields of the test filament are given in Equations (A.5), (A.6) and (A.7) and the magnetic current density of the expansion filament is given by

$$\underline{M}_t = \hat{t}\ \frac{\gamma\cosh\gamma(t-t_m)}{2\sinh\gamma w_t}\ , \qquad \text{(C.48)}$$

where $t_m=(t_2+t_1)/2$ and $w_t=(t_2-t_1)/2$. Combining Equations (A.6), (A.7) and (C.48), the mutual impedance is given by

$$z_{mn}^{MM} = \int_{t_1}^{t_2} \frac{\gamma\cosh\gamma(t-t_m)}{2\sinh\gamma w_t}\left(\frac{x}{\rho}\sin\psi H_\rho + \cos\psi H_z\right) dt\ . \qquad \text{(C.49)}$$

Just as was the case for electric filaments, the mutual impedance between the expansion current and the magnetic test point charges at the ends of the test filament will be computed separately.

Non-planar skew filaments: Expanding Equation (C.49) with Equations (A.6) and (A.7) (end charges removed) gives

$$z_{mn}^{MM} = \frac{\gamma^2}{32\pi n \sinh\gamma w_t \sinh\gamma w_s} \int_{t_1}^{t_2} (e^{\gamma(t-t_m)} + e^{-\gamma(t-t_m)})$$

$$\cdot \left[\frac{x\sin\psi}{\rho^2} \left((\cosh\gamma w_s + \frac{z-z_1}{R_1} \sinh\gamma w_s) e^{-\gamma R_1} \right.\right.$$

$$\left. - (\cosh\gamma w_s - \frac{z-z_2}{R_2} \sinh\gamma w_s) e^{-\gamma R_2} \right)$$

$$\left. - \cos\psi \sinh\gamma w_s \, (e^{-\gamma R_1}/R_1 + e^{-\gamma R_2}/R_2) \right] dt \qquad (C.50)$$

where

$$R_i = \sqrt{z_i^2 + t^2 - 2z_i t \cos\psi + d^2} \quad . \qquad (C.51)$$

Using the same method as for two non-planar skew electric filaments, Equation (C.50) can be evaluated as

$$z_{mn}^{MM} = \frac{-\gamma^2}{64\pi n \sinh\gamma w_s \sinh\gamma w_t} \left[e^{\gamma t_m} (\cosh\gamma w_s (F_1^- - F_2^-) + e^{-\gamma z_m} G_1^- \right.$$

$$\left. + e^{\gamma z_m} G_2^-) + e^{-\gamma t_m} (\cosh\gamma w_s (F_1^+ - F_2^+) + e^{-\gamma z_m} G_1^+ + e^{\gamma z_m} G_2^+) \right] \qquad (C.52)$$

where F_i^s and G_i^s are defined in Equation (C.17).

Parallel filaments: If the filaments are parallel ($\sin\psi=0$), then Equation (C.49) can be expanded with Equations (A.6) and (A.7) (end charges removed) to give

$$z_{mn}^{MM} = \frac{-\gamma^2\cos\psi}{32\pi\eta\sinh\gamma w_t} \int_{t_1}^{t_2} (e^{\gamma(t-t_m)} + e^{-\gamma(t-t_m)})(e^{-\gamma R_1}/R_1 + e^{\gamma R_2}/R_2)dt \tag{C.53}$$

where

$$R_i = \sqrt{(t-z_i\cos\psi)^2 + d^2} \quad , \; i = 1,2, \; \cos\psi = \pm 1 \; . \tag{C.54}$$

Using the same method as for two parallel electric filaments, Equation (C.53) can be evaluated as

$$z_{mn}^{MM} = \frac{-\gamma^2\cos\psi}{32\pi\eta\sinh\gamma w_t} \Bigg|_{-}^{-} e^{\gamma(t_m-z_2\cos\psi)} E(x_2^-) + e^{\gamma(t_m-z_1\cos\psi)} E(x_1^-) - e^{-\gamma(t_m-z_2\cos\psi)} E(x_2^+) - e^{-\gamma(t_m-z_1\cos\psi)} E(x_1^+) \Bigg|_{-}^{-} \tag{C.55}$$

where the E function is defined in Equations (C.13) and (C.14) and the integration interval is

$$x_i^s = R_i - s(t-z_i\cos\psi) \tag{C.56}$$

with R_i as defined in Equation (C.54), $i = 1,2$ and $s = \pm 1$.

Point charge contribution: From Equations (A.6)and (A.7) , the magnetic field due to the point charges at the endpoint of the test magnetic filament are

$$\underline{H}_s = \frac{\cosh\gamma w_s}{8\pi n \sinh\gamma w_s} \left[\hat{R}_2(1+\gamma R_2)e^{-\gamma R_2}/R_2^2 - \hat{R}_1(1+\gamma R_1)e^{-\gamma R_1}/R_1^2 \right] \quad (C.57)$$

where $\hat{R}_i = \hat{\rho}\sin\theta_i + \hat{z}\cos\theta_i$ is a unit vector pointing from the point charge at z_i to the field point. Combining Equations (C.48) and (C.57), the point charge contribution of the mutual impedance of two magnetic filaments is

$$z_{mn}^{MM} = \frac{\gamma\cosh\gamma w_s}{16\pi n \sinh\gamma w_s \sinh\gamma w_t} \int_{t_1}^{t_2} \cosh\gamma(t-t_m) \left[(\hat{t}\cdot\hat{R}_2)(1+\gamma R_2)\, e^{-\gamma R_2}/R_2^2 - (\hat{t}\cdot\hat{R}_1)(1+\gamma R_1)\, e^{-\gamma R_1}/R_1^2 \right] dt \quad (C.58)$$

with

$$R_i = \sqrt{(t-z_i\cos\psi)^2 + (z_i\sin\psi)^2 + d^2} \quad . \quad (C.59)$$

Using the same method as for determining the point charge contribution of the mutual impedance for two electric filaments, Equation (C.58) can be evaluated as

$$Z_{mn}^{MM} = \frac{-\gamma \cosh \gamma w_s}{32\pi n \sinh \gamma w_s \sinh \gamma w_t} \left[\frac{2\cosh \gamma w_t}{\gamma} \left(e^{-\gamma R_1(t_1)}/R_1 - e^{-\gamma R_1(t_2)}/R_1(t_2) \right.\right.$$

$$\left. - e^{-\gamma R_2(t_1)}/R_1 + e^{-\gamma R_2(t_2)}/R_2(t_2) \right)$$

$$+ e^{\gamma(t_m - z_2 \cos\psi)} E(x_2^-) - e^{\gamma(t_m - z_1 \cos\psi)} E(x_1^-)$$

$$\left. + e^{-\gamma(t_m - z_2 \cos\psi)} E(x_2^+) - e^{-\gamma(t_m - z_1 \cos\psi)} E(x_1^-) \right] \qquad (C.60)$$

where the E function is defined in Equations (C.13) and (C.14) and the integration interval is

$$x_i^s = R_i - s(t - z_i \cos\psi) \qquad (C.61)$$

with R_i as defined in Equation (C.59).

REFERENCES

[1] Aviation Week and Space Technology, p. 102, September 14, 1981.

[2] E.H. Newman, "A Surface Patch Model for Polygonal Plates", IEEE Trans on Antennas and Propagation", Vol. AP-30, pp. 588-593, July 1982.

[3] N.N. Wang, J.H. Richmond and M.C. Gilbreath, "Sinusoidal Reaction Formulation for Radiation and Scattering from Conducting Surfaces", IEEE Trans. Antennas Propagation, Vol. AP-23, pp. 376-382, May 1975.

[4] E.H. Newman and D.M. Pozar, "Electromagnetic Modeling of Composite Wire and Surface Geometries", IEEE Trans. Antennas Propagation, Vol. AP-26, pp. 784-789, November 1978.

[5] D.L. Knepp and J. Goldhirsh, "Numerical Analysis of Electromagnetic Radiation Properties of Smooth Conducting Bodies of Arbitrary Shape", IEEE Trans. Antenna Propagation, Vol. 20, pp. 383-388, May 1972.

[6] N.C. Albertsen, J.E. Hansen and N.E. Jensen, "Computation of Radiation from Wire Antennas on Conducting Bodies", IEEE Trans. Antennas Propagation, Vol. AP-22, pp. 200-206, March 1974.

[7] G.J. Burke and A.J. Poggio, "Numerical Electromagnetic Code (NEC) - Method of Moments", Naval Ocean Systems Center, Tech. Doc. 116, AFWL-TR-76-320, July 1977.

[8] J.J.H. Wang, "Numerical Analysis of Three-Dimensional Arbitrarily-Shaped Conducting Scatterers by Trilateral Surface Cell Modelling", Radio Science, Vol. 13, pp. 947-952, November-December 1978.

[9] D.R. Wilton, S.S.M. Rao and A.W. Glisson, "Electromagnetic Scattering by Surfaces of Arbitrary Shape", IEEE Trans. on Antennas and Propagation, Vol. AP-30, pp. 409-418, May 1982.

[10] J. Singh and A.T. Adams, "A Nonrectangular Patch Model for Scattering from Surfaces", IEEE Trans. Antennas Propagation, Vol. AP-27, pp. 531-535, July 1979.

[11] E.H. Newman and D.M. Pozar, "Considerations for Efficient Wire/Surface Modeling", IEEE Trans. Antennas Propagation, Vol. AP-28, pp. 121-125, January 1980.

[12] E.H. Newman, "A User's Manual for Electromagnetic Surface Patch Code (ESP)," Report 713402-1, July 1981, The Ohio State University ElectroScience Laboratory, Department of electrical Engineering; prepared under Contract No. DAAG39-81-K-0020 for the Department of the Army, U.S. Army Research Office, Research Triangle Park, North Carolina.

[13] P. Alexandropoulos, "Computer Modeling of Arbitrary Surfaces by Polygonal Plates and Wires", Master's Thesis, 1983, The Ohio State University, Department of Electrical Engineering.

[14] D.S. Jones, The Theory of Electromagnetism, Chapter 8, MacMillan, New York, 1964.

[15] K.K. Mei, "Unimoment Method of Solving Antenna and Scattering Problems", IEEE Trans. on Antennas and Prop., Vol. AP-22, pp. 760-766, November 1982.

[16] D.R. Wilton and R. Mittra, "A New Numerical Approach to the Calculation of Electromagnetic Scattering Properties of Two-Dimensional Bodies of Arbitrary Cross Section", IEEE Trans. on Antennas and Prop., Vol. AP-20, pp. 310-317, May 1972.

[17] P.C. Waterman, "Matrix Formulation of Electromagnetic Scattering", Proc. IEEE, Vol. 53, pp. 805-812, August 1965.

[18] J.H. Richmond, "Scattering by a Dielectric Cylinder of Arbitrary Cross Section Shape", IEEE Trans. on Antennas and Prop., Vol. AP-13, pp. 334-341, May 1965.

[19] R.F. Harrington and J.R. Mautz, "An Impedance Sheet Approximation for Thin Dielectric Shells", IEEE Trans. on Antennas and Prop., Vol. AP-23, pp. 531-534, July 1975.

[20] E.H. Newman and P. Tulyathan, "Wire Antennas in the Presence of Dielectric/Ferrite Inhomogenity", IEEE Trans. on Antennas and Prop., Vol. AP-26, pp. 587-593, July 1978.

[21] D.P. Nyquist, K.M. Chen and B.S. Guru, "Coupling Between Small Thin-wire Antennas and a Biological Body", IEEE Trans. on Antennas and Prop., Vol. AP-25, pp. 863-865, November 1977.

[22] Y. Chang and R.F. Harrington, "A Surface Formulation for Characteristic Modes of Material Bodies", IEEE Trans. on Antennas and Prop., Vol. AP-25, pp. 789-795, November 1977.

[23] T.K. Wu and L.L. Tsai, "Scattering by Arbitrarily Cross-Sectioned Layered Lossy Dielectric Cylinders", IEEE Trans. on Antennas and Prop., Vol. AP-25, pp. 789-795, November 1977.

[24] A.J. Poggio and E.K. Miller, Computer Techniques for Electromagnetics, Edited by R. Mittra, Oxford: Pergamon, Chapter 4, "Integral Equation Solutions of Three-Dimensional Scattering Problems", 1973.

[25] R.F. Harrington, Field Computations by Moment Methods, New York: MacMillan, 1968.

[26] E.H. Newman and P. Tulyathan, "Analysis of Microstrip Antennas Using Moment Methods", IEEE Trans. on Antennas and Prop., Vol. AP-29, pp. 47-53, January 1981.

[27] T.B.A. Senior, "Backscattering from Resistive Strips", IEEE Trans. on Antennas and Prop., Vol. AP-27, pp. 808-813, November 1979.

[28] R.H. Harrington, Time-Harmonic Electromagnetic Fields, McGraw-Hill, New York, Chapter 3, 1961.

[29] V.H. Rumsey, "Reaction Concept in Electromagnetic Theory", Physical Review, Vol. 94, pp. 1483-1491, June 1954.

[30] J.A. Stratton, Electromagnetic Theory, McGraw-Hill, New York, pp. 511-513, 1941.

[31] J.D. Kraus and K.R. Carver, Electromagnetics, McGraw-Hill, New York, pp. 496-501, 1973.

[32] T.B.A. Senior, "Approximate Boundary Conditions", IEEE Trans. on Antennas and Prop., Vol. AP-29, pp. 826-829, September 1981.

[33] E.H. Newman and M.R. Schrote, "On the Current Distribution for Open Surfaces", IEEE Trans. on Antennas and Prop., Vol. AP-31 pp. 515-518, May 1983.

[34] H.L. Thal and J.F. Finger, "Scattering by Dielectric Containers", IEEE Trans. on Antennas and Prop., Vol. AP-18, pp. 709-711, September 1970.

[35] J.H. Richmond, "Scattering by Dielectric and Conducting Dipoles with Circular and Rectangular Cross Sections", Report 3754-2, April 1974, The Ohio State University ElectroScience Laboratory, Department of Electrical Engineering; prepared under Contract No. N00140-74-C-6017 for the Naval Regional Procurement Office.

[36] S.A. Schelkunoff and H.T. Friis, Antennas Theory and Practice, Wiley, New York pp. 370-401, 1952.

[37] D.M. Pozar, "On Moment Method Solutions for Plate and Wire Geommetries", Ph.D. Dissertation, 1980, The Ohio State University Department of Electrical Engineering.

[38] J.H. Richmond and N.H. Geary, "Mutual Impedance of Nonplanar-Skew Sinusoidal Dipoles", IEEE Trans. on Antennas and Prop., Vol. AP-23, pp. 412-414, May 1975.

[39] H.E. King, "Mutual Impedance of Unequal Length Antennas in Echelon", IRE Trans. on Antennas and Prop., Vol. AP-5, pp. 306-313, July 1957.

[40] J.H. Richmond, private communication, March 1982.